

**Part III**  
**Theoretical Approaches**



## 13 Poisson–Nernst–Planck Theory of Ion Permeation Through Biological Channels

Rob D. Coalson and Maria G. Kurnikova

### 13.1 Introduction

The kinetics of an assembly of charged particles such as electrons, ions, or colloids, particularly when subjected to externally applied electric fields, has been of interest for many years and in many disciplines. In applied physics and electrical engineering, the motion of electrons and holes through semiconductor materials under the influence of an applied voltage plays an essential role in the function of modern electronic components such as transistors, diodes, and infrared lasers (Peyghambarian et al., 1993). Electrochemistry deals in large part with the motion of simple inorganic ions (e.g.,  $\text{Na}^+$ ,  $\text{Cl}^-$ ) in electrolytic solutions and how this motion is influenced when electrodes are employed to generate an electric potential drop across the solution or a membrane interface (Bockris and Reddy, 1998). Larger macroions such as charged polystyrene spheres (radius 0.1–1 micron) can also be manipulated using applied electric fields (Ise and Yoshida, 1996). Many processes in molecular biology, from self-assembly of DNA strands into bundles (Wissenburg et al., 1995) to enzyme-ligand docking (Gilson et al., 1994), are steered by electrostatic forces between biological macroions which are mediated by the response of simple salt ions in the solution.

One particularly intriguing type of biological process that falls into this general category is the flow of ions ( $\text{Na}^+$ ,  $\text{Cl}^-$ ,  $\text{K}^+$ ,  $\text{Ca}^{++}$ , etc.) through pores in lipid bilayer membranes. Lipid bilayers (Fig. 13.1) form the cell membrane as well as internal compartments, called organelles, in eukaryotic cells. The interior of a lipid bilayer, composed of alkane chains, is hydrophobic, and hence ions (being hydrophilic) cannot penetrate through it. Since many bioenergetic processes rely on separating charge across bilayer membranes and then transducing the energy thus stored, it is imperative that there be a mechanism for moving ions across these membranes in a controllable fashion. Nature has solved this problem by developing proteins which are, very roughly, cylindrical channels (pipes) possessing an aqueous pore. They insert themselves into the lipid bilayer, spanning it in a transverse fashion, so that ions can flow through the aqueous pore from one side of the membrane to the other (Fig. 13.1) when driven by an electrochemical gradient. Protein channels are extraordinary devices (Hille, 1992). In many cases, they can be opened and closed to the flow of ions reliably and reversibly by a specific stimulus (e.g., the binding

**Rob D. Coalson and Maria G. Kurnikova**

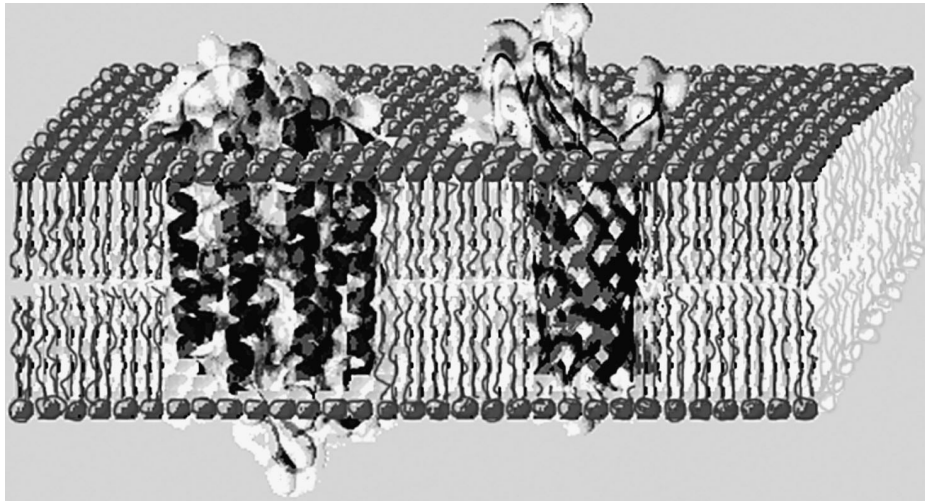


**Fig. 13.1** Schematic picture of lipid bilayer with ion channel proteins in it.

of a specific molecule to the channel protein, or a change in the voltage across the membrane). Furthermore, in the open state, many ion channels are selective about the ions that they let through, sometimes passing only cations but not anions (or vice versa), or even allowing, for example,  $K^+$  but not  $Na^+$  to permeate.

In this review [which is an extension of a recent review on the same general topic (Coalson and Kurnikova, 2005)], we will consider the passage of ions through a protein channel in its open state. We seek to provide a practical solution to the following basic problem. Given the structure of the channel protein (and an estimation of the geometric features of the lipid bilayer), plus some details of the electrical properties of these objects (distribution of electrical charges in them and characteristic dielectric constants), we wish to compute the rate of ion flow through the channel as a function of experimentally controllable parameters, e.g., electric potential applied across the membrane and concentration of ions in the bathing solutions on either side of the membrane. That is, we want to calculate current–voltage ( $I$ – $V$ ) curves for the system at hand. There are several possible approaches that might be envisaged, including (if possible) all-atom molecular dynamics (MD) simulation (Crozier et al., 2001a,b; Aksimentiev and Schulten, 2005) and Brownian Dynamics (Chung et al., 1998, 1999, 2002; Graf et al., 2000; Mashl et al., 2001; Chung and Kuyucak, 2002; Burykin et al., 2002; Im and Roux, 2002; Graf et al., 2004; Noskov et al., 2004; Cheng et al., 2005) simulation of the ion motion. Here we concentrate on the simplest (most coarse-grained) level of treatment imaginable, namely a continuum electrodiffusion model in which the mobile ions are treated as a concentration profile whose distribution and motion are influenced by electrostatic forces (some of which are generated by the polarization of the mobile ion density). In the context of ion permeation through channel proteins, this approach is known as Poisson–Nernst–Planck (PNP) theory. In the next sections, we will present the basic ingredients of

### 13. Poisson–Nernst–Planck Theory of Ion Permeation

this theory as well as techniques for solving the relevant equations that comprise it. Fundamental limitations of the continuum electrodiffusion model (of which there are many!) will be discussed. Some illustrative applications will be presented. Attempts to improve the basic PNP theory will be reviewed. Finally, conclusions and prognosis for this type of analysis will be presented.

## 13.2 Basic (Primitive) PNP Theory (and Its Limitations)

### 13.2.1 The PNP Equations

In continuum theory electrolyte ions are treated as a continuous charge distribution characterized by the concentrations  $\{c_i(\vec{r})\}$  of the ionic species (labeled by  $i$ ) involved. It is the goal of electrodiffusion theories to determine the steady state concentrations of all mobile ion species, the electric fields they generate, and in the context of biological ion channels, the current of ions flowing through the channel as a function of experimentally controllable parameters such as the bulk concentrations of ions (electrolytes) and the electric potential applied across the embedding membrane, usually by means of a microelectrode apparatus. In the present subsection we will collect the working formulae that result from this approach, known generically as PNP theory. In Section 13.2.2, we will explore the conceptual underpinnings of this type of theory.

In electrodiffusion theory, the distribution of mobile ion concentrations is governed by a set of drift–diffusion equations, also called Nernst–Planck (NP) equations, one for each ionic species  $i$  present in solution. In particular,  $\vec{j}_i$ , the flux of species  $i$  at a given point in space is given by

$$\vec{j}_i(\vec{r}) = -D_i(\vec{r}) \left[ \frac{\partial c_i(\vec{r})}{\partial \vec{r}} + c_i(\vec{r}) \frac{\partial}{\partial \vec{r}} (\beta \psi_i(\vec{r})) \right], \quad (13.1a)$$

and the concentration of species  $i$  evolves in accordance with the continuity equation  $\frac{\partial c_i}{\partial t} = -\text{div} \vec{j}_i$ . In Eq. 13.1a,  $D_i$  is the position-dependent diffusion coefficient of species  $i$ ,  $\beta = (kT)^{-1}$  is the inverse temperature,  $k$  is the Boltzmann constant, and  $T$  is the absolute temperature. Finally,  $\psi_i(\vec{r})$  is the free energy of ions of species  $i$  in solution. At steady state,

$$\text{div} \vec{j}_i = 0, \quad (13.1b)$$

and thus all quantities in the NP equation (Eq. 13.1) are time-independent. The second term on the right-hand side of (Eq. 13.1a) is the drift term due to the forces acting on a charged particle of species  $i$  from both ion–ion interactions and other sources. The latter include interactions with charges on the protein system and the externally imposed electric field. Equation 13.1 is supplemented by concentration boundary conditions that account for the external bulk ionic concentrations of species  $i$  (which

## Rob D. Coalson and Maria G. Kurnikova

may be different on different boundary “faces,” particularly if concentrations in the bathing solutions on the two sides of the membrane differ).

In a continuum model,  $\psi_i(\vec{r})$  depends on the electrostatic charge distribution in the system and on the (generally position dependent) dielectric response function  $\epsilon(\vec{r})$ . It is convenient to separate the ion free energy into two contributions:

$$\psi_i(\vec{r}) = q_i \phi_{\text{mobile}}(\vec{r}) + \Delta G_{\text{SIP}}^i(\vec{r}), \quad (13.2)$$

where  $q_i$  is the charge of an ion of species  $i$ ,  $\phi_{\text{mobile}}(\vec{r})$  is the electrostatic potential due to all mobile ions and the applied electric field associated with external electrodes, and  $\Delta G_{\text{SIP}}^i(\vec{r})$  is the potential of mean force (PMF) (McQuarrie, 1976; Chandler, 1987) for a single test ion [hence “Single Ion Potential” (SIP)]. In an inhomogeneous dielectric medium  $\phi_{\text{mobile}}(\vec{r})$  is determined by the Poisson equation<sup>1</sup> (PE):

$$\vec{\nabla} \cdot (\epsilon(\vec{r}) \vec{\nabla} \phi_{\text{mobile}}(\vec{r})) = -4\pi \sum_i q_i c_i(\vec{r}), \quad (13.3)$$

subject to Dirichlet boundary conditions, i.e., values of the electrostatic potential (imposed by the electrodes) are fixed on the boundaries of the computational box (Kurnikova et al., 1999). In the simplest approximation that was introduced in the field of channel modeling by Eisenberg and coworkers (Barcilon, 1992) the term  $\Delta G_{\text{SIP}}^i(\vec{r})$  is disregarded. In an obvious generalization  $\Delta G_{\text{SIP}}^i(\vec{r})$  may include the electrostatic potential due to partial charges fixed on the protein and lipid atoms, i.e.,  $\Delta G_{\text{SIP}}^i(\vec{r}) = q_i \phi_{\text{protein}}(\vec{r})$  (Chen and Eisenberg, 1993a,b; Kurnikova et al., 1999; Cárdenas et al., 2000). Equations 13.1 and 13.3 are coupled nonlinearly via the  $c_i$  and  $\phi_{\text{mobile}}$  variables. In the general case of a protein of arbitrary geometry and distribution of partial charges on protein atoms, these equations have no analytical solution and must be solved numerically to self-consistency (Kurnikova et al., 1999). Equations 13.1–13.3 with  $\Delta G_{\text{SIP}}^i(\vec{r}) = q_i \phi_{\text{protein}}(\vec{r})$  comprise the standard PNP theory, which we shall refer to here as “primitive PNP” for reasons that will become obvious in the ensuing exposition.

### 13.2.2 Conceptual Framework of PNP Theory

Let us consider for the moment a somewhat simpler problem, namely motion of a structureless particle in an external force field  $\vec{F}(\vec{r})$  derivable from a potential energy function  $V(\vec{r})$ , i.e.,  $\vec{F}(\vec{r}) = -\partial V(\vec{r})/\partial \vec{r}$ . The particle is also subject to thermal agitation arising from incessant buffeting by other particles in the system. In the classic theory of Brownian motion (Chandrasekhar, 1943), the Brownian particle (the one whose motion we are explicitly tracking) is much larger than that of tiny particles which are colliding with it. For example, the Brownian particle might be

<sup>1</sup> In equation (Eq. 13.3) CGS Gaussian units are employed. To write the Poisson equation in SI units, substitute  $4\pi \rightarrow 1/\epsilon_0$  on the r.h.s., with  $\epsilon_0$  being the permittivity of free space (Kittel, 1996).

### 13. Poisson–Nernst–Planck Theory of Ion Permeation

a colloid sphere (radius ca. 1 micron), with water molecules (molecular radius of a few Å) bouncing off of it in a rapid and stochastic fashion. When Brownian motion theory is applied to describe motion of one “tagged” atom, ion or small molecule in a condensed phase consisting of other such species, the separation of distance scales inherent in classic Brownian motion theory is not so clear. Nevertheless, this description seems to be quite successful for describing molecular level kinetics in many cases [e.g., the description of ion diffusion in bulk liquids (Mamonov et al., 2003)].

Assuming that Brownian motion theory can be applied to the case of interest, then in the high friction limit the probability distribution for the position of the Brownian particle (or, equivalently, the concentration profile achieved by a collection of such independently moving particles) is given by:

$$\frac{\partial c(\vec{r}, t)}{\partial t} = -\text{div}(\vec{j}) \quad (13.4a)$$

with particle flux

$$\vec{j}(\vec{r}) = -D(\vec{r}) \left[ \frac{\partial c(\vec{r})}{\partial \vec{r}} + c(\vec{r}) \frac{\partial}{\partial \vec{r}} (\beta V(\vec{r})) \right] \quad (13.4b)$$

Here all symbols have the same meaning as in Section 13.2.1 above, except for the obvious substitution of the potential energy function  $V(\vec{r})$  for the more complicated (and mysterious) free energy function invoked in Eq. 13.1a. (For now we will suppress the subscript that labels ion species and speak simply of the behavior of a generic species moving under a generic single-particle force-field). Equation 13.4 is known as the Smoluchowski equation (Chandrasekhar, 1943). The first term contributing to the flux (cf. Eq. 13.4b) is simply the concentration gradient that constitutes Fick’s Law of diffusion. The second term, the so-called “drift” term, represents the influence of the systematic force  $\vec{F}(\vec{r})$ . Consistent with the high-friction assumption underlying the Smoluchowski equation, we imagine that at each point along its trajectory the Brownian particle is damped by the appropriate friction force characterized by friction constant  $\gamma$  and instantaneously reaches its terminal velocity  $\vec{v}_{\text{term}} = \vec{F}/\gamma = \beta D \vec{F}$ . [Here we assume that the Stokes–Einstein relation  $D = kT/\gamma$  connecting microscopic friction to macroscopic diffusion applies (McQuarrie, 1976)]. The flux associated with this drift process is thus  $\vec{j}_{\text{drift}} = c \vec{v}_{\text{term}} = \beta D c \vec{F}$ . Since in general the diffusion constant and the systematic force are position-dependent, so is the drift flux, as indicated in the second term on the r.h.s. of Eq. 13.4b. Note one direct consequence of the structure of the drift–diffusion flux prescription given in Eq. 13.4b: the steady state solution to this equation corresponding to zero particle flux, i.e., thermal equilibrium, is simply the Boltzmann probability distribution  $c(\vec{r}) \propto \exp[-\beta V(\vec{r})]$ , as it should be. However, the most general boundary condition implies a *non*-equilibrium steady state, i.e.,

### Rob D. Coalson and Maria G. Kurnikova

a steady-state solution of the Smoluchowski equation (Eq. 13.4) for which  $\vec{j} \neq 0$  identically.

If we regard one permeating ion in the ion channel systems of direct interest in this article as the tagged Brownian particle, then the situation is clearly more complicated than that of Brownian motion of a collection of noninteracting particles all moving in the same static external force field. The tagged ion experiences a force due to each of the other moving ions, and indeed, due to each atom in the protein (and membrane), which are also fluctuating with time. To utilize the Brownian motion theory framework just sketched, we seek to identify an *optimal effective static single particle potential* that can play the role of  $V(\vec{r})$  in Eq. 13.4. In the (temporary) absence of the other mobile ions and the externally applied electrical potential, the most reasonable candidate is the PMF (constrained free energy profile)  $\Delta G_{\text{SIP}}^i(\vec{r})$  for a tagged particle of species  $i$  (McQuarrie, 1976). (We need to recall at this juncture that there are generally two or more ionic species in the electrolyte, each of which experiences different energetic interactions.) The PMF is obtained from the Boltzmann factor for the ion and all water, protein and membrane atoms particles in the system, given in terms of the full many-dimensional microscopic potential energy function  $U_i$  which describes the mutual interactions between these particles, by integrating over all degrees of freedom except those of the ion. Specifically:

make bigger /

$$\exp[-\beta \Delta G_{\text{SIP}}^i(\vec{r})] = \int d\vec{R} \exp[-\beta U_i(\vec{r}, \vec{R})] / \int d\vec{r} \int d\vec{R} \exp[-\beta U_i(\vec{r}, \vec{R})],$$

where  $\vec{R}$  represents all “environmental” coordinates in the system, i.e., those of the water molecules and the atoms in the protein and the membrane. This choice ensures the correct reduced probability distribution (concentration profile), namely  $\exp[-\beta \Delta G_{\text{SIP}}^i(\vec{r})]$ , for the ion at thermal equilibrium taking into account the effects of water solvent and thermal fluctuation of the protein and membrane, but in the absence of ion–ion interactions and the external electric potential. To this effective potential we then add the influence of the applied external electric potential  $\phi_{\text{ext}}(\vec{r})$ , i.e., add the term  $q_i \phi_{\text{ext}}(\vec{r})$  to  $\Delta G_{\text{SIP}}^i(\vec{r})$ . Finally, we need to account for the average force exerted by all other mobile ions in the system on the tagged ion. We assume that these other ions collectively generate an additional electric potential that acts on said ion. ~~Of course~~, these other mobile ions are ~~in fact~~ moving, so their distribution in space with respect to the tagged ion changes with time. We ignore these fluctuations and assume that the static average distribution of the ions other than the test ion can be used to calculate a meaningful time-averaged electric potential  $\phi_{\text{MI}}$  at point  $\vec{r}$ . Further, we replace this conditional probability, i.e., fixing the test ion and averaging over all others, with the average ion density profile (including all ions without any constraints). These are the essential ingredients of a “mean field” approximation. [Similar strategies have long been utilized to understand the thermodynamic properties of ferromagnets (Chandler, 1987) and polymers (Doi, 1996)].

### 13. Poisson–Nernst–Planck Theory of Ion Permeation

Within the context of this approximation,  $\phi_{\text{MI}}$  can be calculated from the steady-state concentration profiles  $c_i(\vec{r})$  characterizing each mobile ion species. In the case of a dielectrically uniform medium characterized by dielectric constant  $\epsilon$ , then  $\phi_{\text{MI}}(\vec{r}) = \int d\vec{r}' \sum_i q_i c_i(\vec{r}') / \epsilon |\vec{r} - \vec{r}'|$ . In fact, biological ion channels are inherently characterized by several spatial regions with different dielectric constants. Hence,  $\phi_{\text{MI}}(\vec{r})$  must be obtained by solving the PE (cf. Eq. 13.3). (The relevant boundary condition for this computation ~~would be~~ zero electric potential on the boundaries of the computational box, since the polarization of  $+/-$  mobile ion charge is confined to the channel region). The complete effective single-particle potential thus becomes:

$$\psi_i(\vec{r}) = \Delta G_{\text{SIP}}^i(\vec{r}) + q_i [\phi_{\text{ext}}(\vec{r}) + \phi_{\text{MI}}(\vec{r})]$$

Since the external electric potential typically supplied by microelectrodes can be computed by solving the Laplace equation [PE with zero free charge (Marion, 1965)] and fixed potential boundary conditions on the walls of the box (with a different potential on the two faces of the computational box which run parallel to the membrane surface), the sum  $(\phi_{\text{ext}} + \phi_{\text{MI}}) \equiv \phi_{\text{mobile}}$  can be obtained by solving a single PE with these “potential” boundary conditions, as specified in Section 13.2.1. Of course, the  $c_i(\vec{r})$  must be obtained by self-consistent solution of both NP and PE equations. Note also that the size of the mobile ions is not taken into account in the mean field averaging procedure invoked here.

The calculation of  $\Delta G_{\text{SIP}}^i(\vec{r})$  is a prequel to the PNP-type calculation just outlined. In principle  $\Delta G_{\text{SIP}}^i(\vec{r})$  can be computed numerically using an all-atom model of the system (test ion, water, protein, and membrane). However, such calculations are quite time-consuming and require a high accuracy force field. In the absence of force fields, which include electronic polarizability effects properly, even recent high-level all atom single ion free energy profiles appear to give unrealistic results (Allen et al., 2004). An alternative strategy is to use semiempirical strategies based wholly or in part on a continuum theory description of the solvent, protein and membrane to obtain  $\Delta G_{\text{SIP}}^i(\vec{r})$  (Mamonov et al., 2003). A hierarchy of increasingly sophisticated strategies of this type will be presented in the course of this article. It is clear from the brief sketch of the “derivation” of PNP above that this type of theory is far from rigorous; the same sketch hopefully suggests ways to remove some of its deficiencies (Schuss et al., 2001; Mamonov et al., 2003; Graf et al., 2004; Gillespie et al., 2005; Wang et al., 2005).

#### 13.2.3 Goldman–Hodgkin–Katz Theory of Ion Permeation Through Channel Proteins

A principal feature of the PNP equations is that the effective potential which enters into the NP equations, and hence determines the steady state concentration profile, is itself a function of the (unknown) concentration of mobile ions, as reflected in the structure of the PE (Eq. 13.3). Thus, as noted above, the NP and PEs must be solved

### Rob D. Coalson and Maria G. Kurnikova

self-consistently, which compounds the difficulty of solving them numerically and may cloud insight into the properties of the resultant solutions (steady state mobile ion distributions, ion currents, etc.). It would certainly be convenient if the effect of mobile ion–mobile ion interactions on the effective potential felt by a “tagged” mobile ion could be neglected, so that the NP equation for that ionic species would be governed by a simple externally prescribed potential energy function, namely:  $V_i(\vec{r}) = \Delta G_{\text{SIP}}^i(\vec{r}) + q_i \phi_{\text{ext}}(\vec{r})$ . One case where it is reasonable to expect such a situation to occur is when the ion channel is so narrow that only one ion is likely to be in it at any particular time. Numerical studies which include multi-ion kinetics at the Brownian dynamics (BD) level (i.e., not assuming a mean-field ion–ion interaction potential as is done in PNP theory) show that in narrow model channels ion–ion interactions have a relatively minor effect on net ion currents (Graf et al., 2000). Then, going one step further, since the ion channels under consideration in this subsection are presumed to be rather narrow, we may as well assume that they are cylindrical in nature with a cylinder radius  $R$  and a small ratio of cylinder radius to cylinder length  $L$  [see, for example, Fig. 1 of Ref. (Kurnikova et al., 1999)]. Because the cylinder is narrow, the potential energy profile inside it can be well-approximated as a function of the channel axis coordinate  $z$  only, i.e.,  $V_i(z)$ . In this situation, the solution of the 3D NP equation yields a concentration profile that also depends only on the channel axis coordinate, and is a solution of the 1D NP equation (Barcilon, 1992; Barcilon et al., 1992). That is, suppressing the ionic species labels for notational convenience:

$$0 = \frac{\partial}{\partial z} \left\{ D(z) \left[ \frac{\partial c(z)}{\partial z} + c(z) \frac{\partial (\beta V(z))}{\partial z} \right] \right\}. \quad (13.5)$$

no  $\pi$

← This differential equation can be solved explicitly for  $c(z)$ , given the values of the concentration at the two boundaries,  $c(0) \equiv c_0$  and  $c(L) \equiv c_L$ . One finds in the case of a spatially homogeneous diffusion constant  $D$  that the current density (aligned with the channel axis) is prescribed by:

$$j = -D \frac{[c_L e^{\beta V_L} - c_0 e^{\beta V_0}]}{\int_0^L dz' e^{\beta V(z')}} \quad (13.6)$$

where  $V(0) \equiv V_0$  and  $V(L) \equiv V_L$ . Thus the problem of computing current flow through this class of simple model channels is reduced to a 1D quadrature for arbitrary  $V(z)$ .

Having simplified the complex phenomenon of ion permeation through a biological channel to this degree, it behooves us to ask what is the simplest meaningful model for  $V_i(z)$  appropriate to ionic species  $i$ . In the absence of the channel (pore) in the membrane, the electric potential drop across the channel would be essentially linear, i.e.,  $\phi_{\text{ext}}(z) = \phi_0 + z(\phi_L - \phi_0)/L$ , where  $\phi(0) = \phi_0$  and  $\phi(L) = \phi_L$  are the values of the applied potential in the reservoirs abutting the channel on either side. (Only the applied potential difference  $\phi_L - \phi_0 \equiv \phi_{\text{ap}}$  is physically meaningful, as

### 13. Poisson–Nernst–Planck Theory of Ion Permeation

is apparent from Eq. 13.6). The channel pore represents only a tiny “pin prick” in the membrane, so we expect that the linear drop approximation remains reasonable inside the channel pore. By construction (of this model), we are ignoring ion–ion interactions. This still leaves the single-ion  $\Delta G_{\text{SIP}}^i(z)$  contribution to  $V_i(z)$ . In an ultra-simple model we can ignore this, assuming that it is small compared to the applied external potential term. We should emphasize that any  $\Delta G_{\text{SIP}}^i(z)$  can be added to the analysis in this section without changing its essential structure. The advantage to neglecting it is that the quadrature in Eq. 13.6 can be analytically computed in the case of the linear potential drop model, which is known historically as the Goldman–Hodgkin–Katz (GHK) model (Hille, 1992; Sten-Knudsen, 1978).

For concreteness, let us further specialize to the case that the bathing solutions consist of a monovalent electrolyte (e.g., NaCl). Then the GHK model predicts current densities for  $+/-$  ions of:

$$j_{\pm} = \frac{\mp D_{\pm} \Delta}{L} \left[ \frac{c_L}{1 - e^{\mp \Delta}} - \frac{c_0}{e^{\pm \Delta} - 1} \right], \quad (13.7)$$

where  $\Delta \equiv e_0 \phi_{\text{ap}} / kT$  and  $e_0$  is the proton charge. Note also that the  $+/-$  ion species may have different effective diffusivities  $D_{\pm}$ , which describe their diffusion within the pore (and may be different in magnitude from their corresponding bulk solution values). To obtain absolute electric currents we simply multiply by the cross-sectional area of the cylinder and the ion charge. If  $i_{\pm}$  is the (particle) current of  $\pm$  ions (i.e., number of particles/sec), then

$$e_0 i_{\pm} \cong \mp 1000 \frac{\pi R^2}{L} D_{\pm} \Delta \left[ \frac{c_L}{1 - e^{\mp \Delta}} - \frac{c_0}{e^{\pm \Delta} - 1} \right]. \quad (13.8)$$

This formula gives as output current in pA, inputting  $D$  in  $\text{cm}^2/\text{s}$ ,  $c$  in mM, and  $R$  and  $L$  in  $\text{\AA}$ . Finally, the experimentally observed electric current is  $I = e_0(i_+ - i_-)$ .

The GHK equations can be used to predict ion current through a channel protein for a wide range of experimental conditions. One such plot is shown in Fig. 13.2 for parameters specified in the figure caption. This figure illustrates several generic characteristics of  $I-V$  curves obtained from GHK theory. In the general case, the current is much greater when the voltage has one sign than it is when the sense of the voltage is reversed, all other things being equal. This phenomenon, known as “rectification,” is observed in many experimental measurements of ion channel  $I-V$  curves. Further, the current grows linearly with large applied voltage, again consistent with many experiments. Finally, the current vanishes at a particular applied voltage, known as the “reversal potential”  $\phi_{\text{rev}}$ . In general  $\phi_{\text{rev}}$  is not zero, but is given, according to GHK theory, by:

$$e^{\Delta_{\text{rev}}} = \frac{D_+ c_0 + D_- c_L}{D_- c_0 + D_+ c_L},$$

Rob D. Coalson and Maria G. Kurnikova

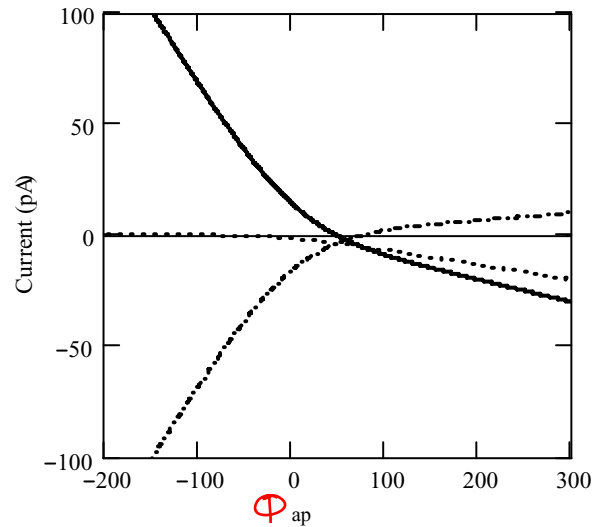


**Fig. 13.2** GHK current–voltage characteristics (solid line) is shown for cylindrical model ion channel system, radius  $R = 2 \text{ \AA}$ ,  $L = 30 \text{ \AA}$  at room temperature ( $T = 298 \text{ K}$ ) characterized by: (internal) diffusion constants  $D_+ = 10^{-5} \text{ cm}^2/\text{s}$ ,  $D_- = 10^{-4} \text{ cm}^2/\text{s}$ , and reservoir concentrations  $c_0 = 20 \text{ mM}$ ,  $c_L = 400 \text{ mM}$ . Also shown are  $e_0 i_+$  (dotted line) and  $e_0 i_-$  (dot–dashed line), given by Eq. 13.8. The observed electrical current (solid line)  $I$  is given by the difference between these, i.e.,  $I = e_0 i_+ - e_0 i_-$ . (Note:  $\phi_{\text{ap}} \cong 25\Delta$  for monovalent ions at room temperature; cf. Eq. 13.8.)

with  $\Delta_{\text{rev}} = e_0 \phi_{\text{rev}}/kT$ . This equation can be rearranged to read:

$$\frac{D_+}{D_-} = \frac{c_0 e^{\Delta_{\text{rev}}} - c_L}{c_0 - c_L e^{\Delta_{\text{rev}}}},$$

which provides a way to calculate the ratio of intrinsic diffusivities of  $+/-$  ions (known as the “permeability ratio”) by measuring the reversal potential experimentally under asymmetric bathing solution conditions.

One other important characteristic of GHK theory (or any 1D NP theory of the type under consideration here) is that the current scales are proportional to the concentrations in the bulk reservoirs. That is, if both  $c_0$  and  $c_L$  double, all other factors being unchanged, then the electric current predicted by the GHK model doubles (cf. Eq. 13.8). This behavior is found experimentally at low bathing solution concentrations, but generally currents are observed to saturate as the concentration of the bathing solutions is increased. The origin of this discrepancy will be discussed in Section 13.6.

This brief survey of 1D NP theory and its application to ion channels in the case of a constant effective driving force (electric field) exposes advantages and disadvantages of GHK theory. The great advantage is the conceptual simplicity of the model and its amenability to analytical solution over a wide range of physical input parameters. But such simplicity comes at a price, namely some loss of realism:

### 13. Poisson–Nernst–Planck Theory of Ion Permeation

GHK theory neglects numerous aspects of the 3D nature of the overall channel system (including the abutting bathing solutions), the atomic (chemical) details of the pore lining, and the interaction forces between all pairs of mobile ions. It is thus interesting to examine how well a fully 3D model of PNP theory, including modifications to primitive PNP theory that attempt to incorporate the effect of protein fluctuations on the permeation of ions through channel proteins, can correct some deficiencies of classical GHK theory. Such an examination is undertaken in the following sections.

#### 13.3 Numerical Algorithms for Solving the 3D PNP Equations

The PNP equations consist of a set of coupled partial differential equations (PDEs), namely the NP equation (Eq. 13.1) (more precisely, one such NP equation for each ionic species), and the PE of electrostatics equation (Eq. 13.3). The 3D NP and the PE can only be solved analytically in a limited number of cases where the system possesses a high degree of geometric symmetry (thus resulting in an effective reduction in dimensionality). In the case of a general 3D system, these PDEs can be solved individually using a variety of numerical methods, two of the most popular being the method of Finite Differences (Kurnikova et al., 1999; Cardenas et al., 2000) and the method of Finite Elements (Hollerbach et al., 2000). For concreteness, we will focus here on the technically simpler Finite Difference approach. For example, the following strategy can be used to solve the 3D PE.

First we discretize onto a 3D cubic lattice an initial guess for the electric potential field (whose computation is the end result of the calculation). In the cases of interest to us the electric potential is specified on the boundaries of the computational box (lattice); it is unknown in the interior of the computational box (our goal is to determine it!). Hence, we set the known boundary values of the electric potential and make an arbitrary initial guess about the field values at the interior points of the lattice. In a similar fashion, we discretize the charge distribution and the spatially dependent dielectric constant profile, which are both assumed to be given. Then, we cycle around the interior lattice: the electric potential  $\phi_k$  at each interior lattice point  $k$  is updated based on an appropriate average over its nearest neighbors (of which there are six for a 3D cubic lattice). For example, in the case where there is no free charge, i.e., the r.h.s. of Eq. 13.3 is identically zero [so that the PE reduces to Laplace equation (Marion, 1965)], and if the dielectric constant  $\epsilon$  is the same everywhere in space, then the update value of the electric potential at lattice point  $k$  is simply the arithmetic average of the potential at the six nearest neighbor sites. If any of these neighbors is a boundary point, its value is known as a boundary condition. Otherwise, the neighboring field points depend on the current field configuration (as the relaxation procedure progresses). In the general case, when there is free charge in the system (the r.h.s. of Eq. 13.3 does not vanish), and the dielectric profile is spatially inhomogeneous, then the relevant average, which is still a linear function

### Rob D. Coalson and Maria G. Kurnikova

of the values of the “instantaneous” potential at the six nearest neighbor sites, is slightly more complicated [see Ref. (Kurnikova et al., 1999) for full details].

If we denote the appropriate average as  $\bar{\phi}_k$ , then the updated value of  $\phi_k$  becomes  $\phi_k \rightarrow w\phi_k + (1-w)\bar{\phi}_k$ , where  $w$  is a parameter (typically  $0 < w < 2$ ) which is adjusted so as to accelerate convergence without sacrificing stability. For  $w$  very small, only a small “portion” of  $\bar{\phi}_k$  is mixed in with  $\phi_k$ , thus preventing numerical instabilities from setting in. This process is repeated for several cycles until no further changes in the potential profile are obtained, i.e., the input potential field at the beginning of the cycle is the same as the output field at the end of the cycle. Strategies of this type are known as “relaxation techniques” (Coalson and Beck, 1998; Press et al., 1986). They are well developed in applied PDE theory. Furthermore, for a linear PDE, such as the PE, relaxation techniques are guaranteed to converge for an arbitrary initial electric potential guess when  $w$  is chosen appropriately.

The NP equation is also a linear PDE. Thus the same relaxation methods can be used to solve it on a cubic grid. In the case of the concentration profile of an ionic species, the values at the external boundaries of the computational box are specified, analogous to the case of fixed electric potential in the PE. In addition, there may be interior walls (e.g., the pore of an ion channel) which do not allow ions to pass through them. The appropriate boundary condition at these interfaces is “zero flux”: this boundary condition can easily be implemented by changing the averaging procedure slightly for interior grid points which abut such bounding surfaces. Analogous to charge and dielectric profile fields in the PE, the spatially-dependent diffusion constant profile as well as the potential energy function which enter into the NP equation must also be discretized, and these become ingredients in the nearest neighbor averaging prescription that is used to update the ion concentration field.

To illustrate the basic strategy, consider (for notational and pictorial simplicity) the 2D, one component analog shown in Fig. 13.3 [reproduced from (Cárdenas et al., 2000)]. Each of the flux contributions can be approximated by an appropriately symmetrized lattice discretization scheme. For example:

$$j_{i+1}^x = -[(D_{i+1,j} + D_{i,j})/2a][c_{i+1,j} - c_{i,j} + \beta(V_{i+1,j} - V_{i,j})(c_{i+1,j} + c_{i,j})/2],$$

where  $a$  is the lattice spacing. Then the lattice version of the NP equation  $\text{div}(\vec{j}) = 0$  is simply  $j_{i+1}^x - j_{i-1}^x + j_{j+1}^y - j_{j-1}^y = 0$ . The procedure for the 3D case is completely analogous: the lattice NP equation can then be rearranged to obtain the concentration of the central lattice point as a linear combination of the concentrations of its six nearest neighbors. Enforcement of zero-flux boundary conditions is done by setting the appropriate lattice flux to zero, thus altering the update formula for the central concentration point in a straightforward manner. For full details, see Refs. (Kurnikova et al., 1999; Cárdenas et al., 2000). The NP equation, like the PE, is a linear PDE, so that convergence of the relaxation technique is virtually guaranteed.

The PNP equations consist of coupled NP equations and a PE. These can only be solved analytically in special cases, namely, when the electric fields generated

### 13. Poisson–Nernst–Planck Theory of Ion Permeation

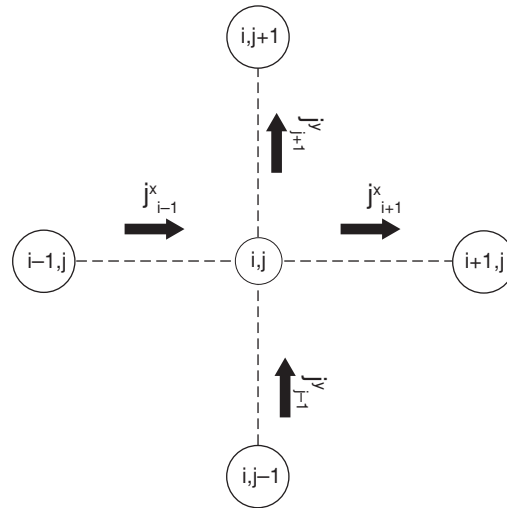


**Fig. 13.3** Schematic description of current flow in/out of lattice point  $i, j$  in a 2D drift–diffusion process.

by mobile ions are small [Debye–Hückel theory being the most familiar example (McQuarrie, 1976)] and there is a degree of geometrical symmetry (as noted above in the case of NP and PEs individually). For the vast majority of interesting physical situations, the PNP equations must be solved numerically. This is done by solving the Poisson and NP equations (one NP equation for each ionic species) numerically and self-consistently. In practice, at each time step we use the current value of the electric potential as a (fixed) input into each NP equation, and vice versa. The coupled PNP equations are nonlinear, and therefore relaxation must be done delicately, using a small value of the weight parameter  $w$  in both NP and PEs. It is found numerically (Kurnikova et al., 1999; Cardenas et al., 2000) that convergence can be obtained in this manner, although the process may be slow (depending on system conditions). Thus, there is room for improvement in the efficiency of numerical procedure, e.g., the use of variable mesh grids and multigrid methodologies.

## 13.4 Application of Primitive PNP to Gramicidin A in Charged/Dipolar Lipid Bilayers

### 13.4.1 The Model System

Gramicidin A (GA) is an antibiotic polypeptide widely used in single-channel experiments on passive ion–current permeation through a lipid membrane. GA is a small 15 amino acid  $\beta$ -helical peptide with an aqueous pore. Due to its unusual primary sequence of alternating L and D amino acids it forms a  $\beta$ -helix with all the amino acid side-groups extending away from the backbone helix, which forms the narrow (ca. 2 Å

### Rob D. Coalson and Maria G. Kurnikova

radius) channel. GA reconstructs into a lipid bilayer by forming head-to-head dimers. Therefore, the channel is lined with backbone carbonyl and amino groups, generating a hydrophilic environment inside the pore, and thus allows cations to flow through it. Its structure has been well-characterized by solution phase NMR (Arsen'ev et al., 1986), and it is readily available in large quantities. Consequently, it has been studied extensively, both experimentally and theoretically. In interesting experiments by Rostovtseva et al. (1998), single channel conductance was measured for GA in several types of lipid bilayers. The lipids used to form these bilayers were characterized by different molecular head groups, which have distinctly different electrostatic characteristics. Phosphatidylcholine (PC) and phosphatidylserine (PS) have dipolar head groups, while, in addition, PS can be charged (due to deprotonation of carboxyl groups on its surface). Busath et al. (Busath et al., 1998) performed similar studies on the uncharged dipolar diphytanoylphosphatidylcholine (DPhPC) membrane and on the uncharged nondipolar glycerilmonoolein (GMO) membrane. The data obtained from these experiments provide valuable information about the role of long-range electrostatic effects on ion permeation through functional protein channels.

#### 13.4.2 Calculations

In an attempt to better understand these issues, an extensive set of 3D ion permeation calculations was performed on these systems (Cárdenas et al., 2000). The geometric details of the lipid (thickness of the bilayer, perturbations of its structure at the regions of contact with the GA, etc.) were modeled based on known structural data (e.g., as obtained from NMR spectroscopy). Following standard arguments (Kurnikova et al., 1999), the dielectric constant of water (both in bulk solvent and in the aqueous pore) was taken to be 2, while that corresponding to protein and membrane regions was set to 80. Charges and dipoles were added as indicated in Fig. 13.4. The individual dipole magnitude and the surface density of dipoles for PC/PS are known. The surface density of titrating surface sites is also known. The degree to which these sites are protonated (and thus electrically neutral) or deprotonated (and thus, characterized by a charge of  $-e_0$ ,  ~~$e_0$  being the proton charge~~) is controlled by experimental conditions (solution pH and electrolyte concentrations): this is a “knob” which can be turned, experimentally, to control the degree of charging of the membrane surface from zero to a maximum (negative) surface charge density equal to the surface density of the titrating acidic (COOH) head groups.

Three-dimensional PNP results for  $I-V$  curves are presented in Figs. 13.5–13.7. The basic physical effects of membrane charge that explain the trends in these curves are as follows. For specified pH and bathing solution salt concentration, and for the same head group dipolar surface density, increasing the “bare” charge on the lipid (by deprotonation of COOH groups) increases the current through the channel. This is because Gramicidin is cation selective and negative surface charge helps attract positive ions in the bulk solution to the surface of the membrane, where they can be “sucked into” the mouth of the ion channel. In contrast, if all other factors are held constant, increasing the dipolar density decreases cation current because of

### 13. Poisson–Nernst–Planck Theory of Ion Permeation

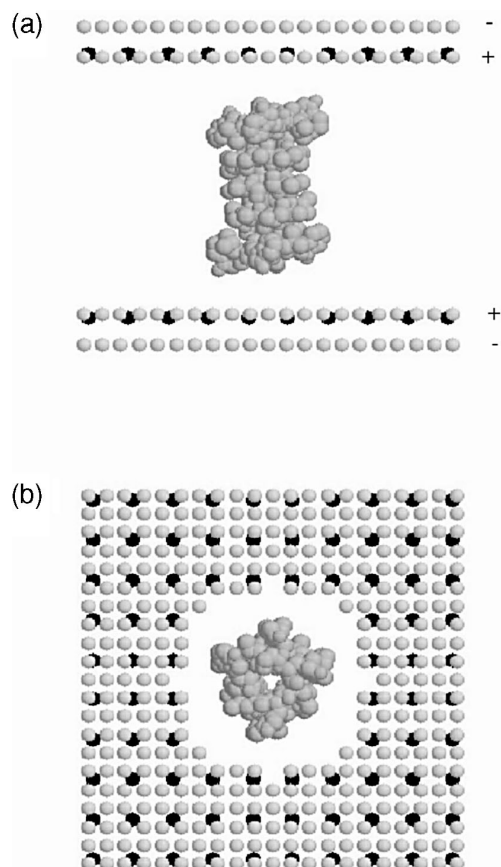


**Fig. 13.4** Molecular representation of the GA dimer with negative charges (black) and dipoles (light gray) embedded in the membrane: (a) lateral view and (b) top view. The negative charges and the positive charges of the dipoles are placed inside the membrane [+ sign in (a)]. The negative charges of the dipoles are placed on the aqueous side of the membrane–liquid interface [–sign in (a)].

the way the dipoles align with respect to the lipid surface: the positive part of the dipole is on the inside, and this positive surface charge presents a (mild) barrier to cation entry into the channel.

Figures 13.5–13.7 compare 3D PNP results to experiment for a variety of systems and conditions. In finalizing the computational output, there is one other critical parameter that needs to be set, namely the constant which governs diffusion within the channel. While the external (bulk) diffusion constants of ions like  $\text{Na}^+$  and  $\text{Cl}^-$  are well known experimentally, the internal diffusion constant has not been measured. Because of the highly restricted motion of both ions and water in a narrow channel like GA, it is plausible that the diffusion constant is significantly lower than its bulk value. There is some support for this conclusion from MD simulations

Rob D. Coalson and Maria G. Kurnikova

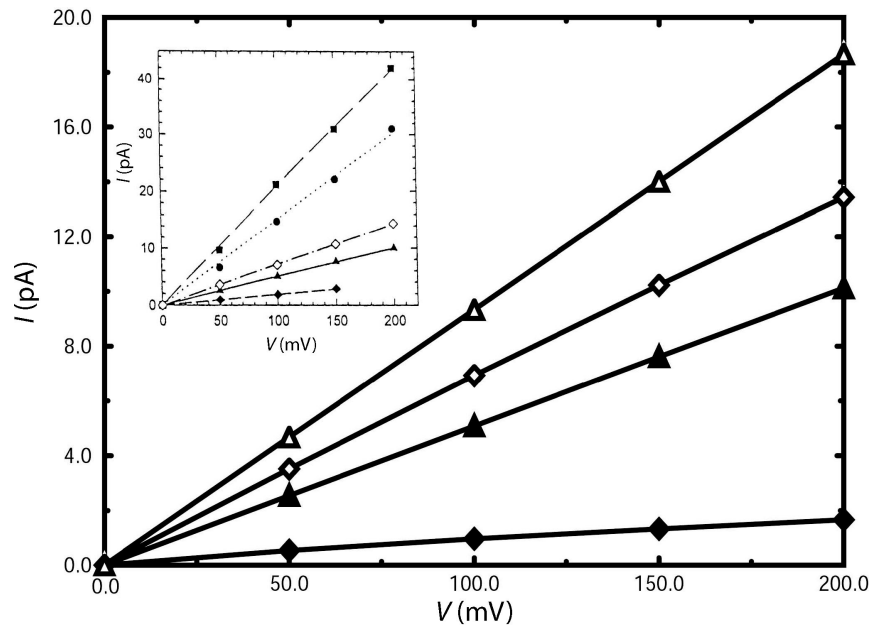


**Fig. 13.5** Calculated current–voltage relationship for GA embedded in an uncharged PC membrane (solid symbols) and a charged PS membrane (open symbols) at neutral pH. The electrolyte concentrations are 0.1 M (diamonds) and 1.0 M (triangles). The inset shows experimental results (Rostovtseva et al., 1998) using the same symbol convention as in the main panel [it also shows experimental results at pH 1 (solid circles and squares)]. The value  $D_{\text{int}} = 1.79 \times 10^{-6} \text{ cm}^2/\text{s}$  was used in these PNP calculations.

in both artificial cavities (Lynden-Bell and Rasaiah, 1996) and in biological ion channels (Mamonov et al., 2003). In any case, it was found empirically that a value of  $D_{\text{int}} \cong 1.5 \times 10^{-6} \text{ cm}^2/\text{s}$  for both anions and cations (about a factor of 10 less than the bulk value for  $\text{K}^+$ ) leads to agreement between 3D PNP theory and experiment which is overall very good. Only in Fig. 13.7, at the high salt concentration of 2M (physiological concentrations of salt rarely exceed 1M), does PNP deviate from experiment significantly. Namely, the experimental current saturates (increasing the salt concentration does not increase the current), while the PNP current does not. This saturation effect is discussed in more detail below.

### 13.5 Incorporating Ion (De)Hydration Energy Effects into PNP: DSEPNP

It was recognized recently, that the change in solvation energy of a single ion when it moves in an inhomogeneous dielectric medium can provide an important contribution to the drift flux term of Eq. 13.1 (Graf et al., 2000; Schuss et al., 2001) but is missing from the primitive PNP definition of  $\Delta G_{\text{SIP}}^i(\vec{r})$ . This change in the free energy of

### 13. Poisson–Nernst–Planck Theory of Ion Permeation

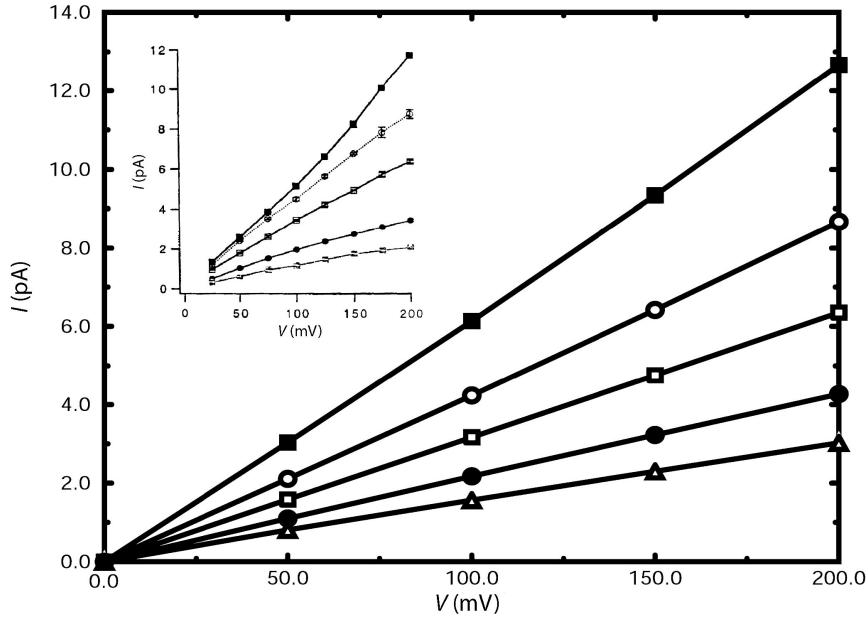


**Fig. 13.6** Current–voltage relationship in GMO (nondipolar) membrane. The electrolyte concentrations are 0.1 (open triangle), 0.2 (closed circle), 0.5 (open square), 1.0 (open circle) and 2.0 M (closed square). The inset shows the experimental results (Busath et al., 1998) with the same symbol convention, except that these authors used dot-filled squares for 0.1 M. The value  $D_{\text{int}} = 1.12 \times 10^{-6} \text{ cm}^2/\text{s}$  was used in these PNP calculations.

a single ion defined with respect to the free energy of that ion in a bulk solvent was termed as the dielectric self-energy (or dielectric barrier)  $\Delta G_{\text{DSE}}^i(\vec{r})$  (Graf et al., 2000, 2004). It can be calculated by solving the 3D PE for an ion with its center placed at one of the lattice points and, from the resultant electric potential field, evaluating the electrostatic energy of this point charge in the appropriate dielectric medium; the procedure is then repeated for all lattice points to map out the spatial dependence of the DSE [see (Dieckmann et al., 1999; Graf et al., 2000) for computational details]. When this contribution to the free energy is taken into account,  $\Delta G_{\text{SIP}}^i(\vec{r})$  is modified to

$$\Delta G_{\text{SIP}}^i(\vec{r}) = q_i \Phi_{\text{protein}}(\vec{r}) + \Delta G_{\text{DSE}}^i(\vec{r}). \quad (13.9)$$

Recent studies have shown that  $\Delta G_{\text{DSE}}^i$  in a narrow channel strongly influences the resulting current (Graf et al., 2000, 2004). Therefore, a careful assessment of  $\Delta G_{\text{SIP}}^i(\vec{r})$  is essential for modeling realistic channel behavior. PNP-like theory that implements  $\Delta G_{\text{SIP}}^i(\vec{r})$  as defined in Eq. 13.4 will be termed Dielectric Self Energy–Poisson–Nernst–Planck (DSEPNP) theory (Graf et al., 2004). Comparison of 3D PNP and DSEPNP calculations to BD simulations in model cylindrical ion channel systems (cf. Fig. 13.8) shows that the simple procedure of adding the single-particle

Rob D. Coalson and Maria G. Kurnikova

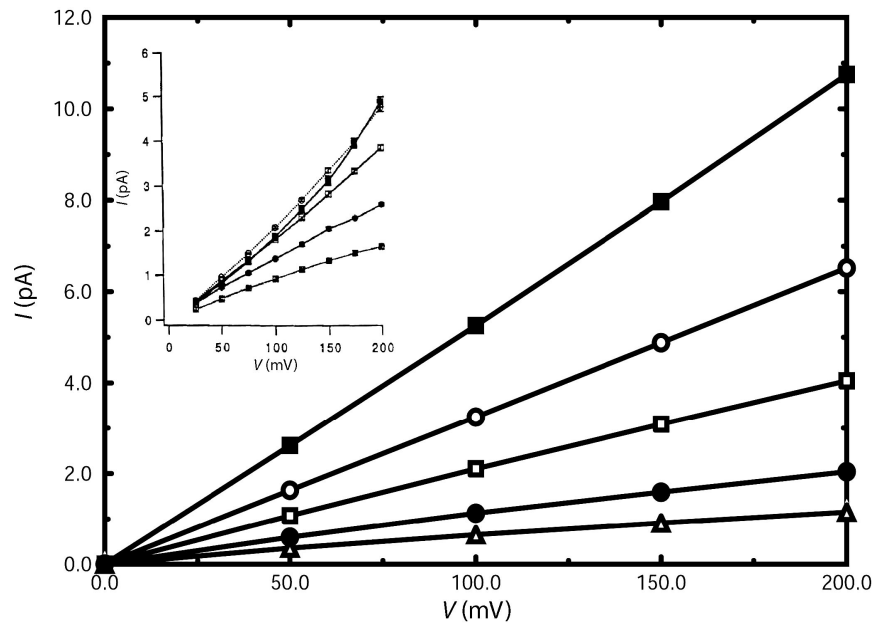


**Fig. 13.7** Current–voltage relationship in DPhPC (dipolar) membrane. The symbol legend is the same as in the previous figure. The experimental results (Busath et al., 1998) are shown in the inset. The value  $D_{\text{int}} = 1.12 \times 10^{-6} \text{ cm}^2/\text{s}$  was used in these PNP calculations.

DSE term to the effective potential in the drift flux term of the PNP equations accounts, at least in these systems, for nearly the entire error inherent in the PNP. The BD model considers the same protein/membrane system, except that all the mobile ions are treated as spherical particles of finite size; water is again treated as a dielectric continuum, and the protein/membrane as an impenetrable dielectric medium. Each ion interacts with the electric field created by fixed ions in the protein/membrane slab, induced charge on dielectric boundaries, and with other ions in a pair-wise additive manner (this pair potential in general differs from a simple Coulomb potential—it is also modulated by induced charge at dielectric interfaces), as well as with the external electric field generated by electrodes. Full details of the calculation of the instantaneous electrostatic force on each ion and the relevant kinetics algorithm used to produce the BD results shown in the present example may be found in (Graf et al., 2000).

Once the DSE potential is restored into PNP theory, the only “approximate” element in it, relative to a full many-ion BD simulation, is the mean-field approximation to ion–ion interactions. From the results shown in Figs. 13.9–13.10 it appears that this approximation is surprisingly accurate. Of course, further testing will be required to determine its full range of validity (Corry et al., 2003).

### 13. Poisson–Nernst–Planck Theory of Ion Permeation

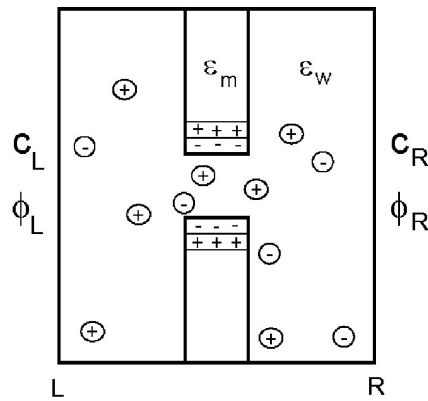


**Fig. 13.8** 2D cross section of the 3D BD simulation box depicting an assembly of free charges in a dielectrically inhomogeneous medium ( $\epsilon_m$  = protein/membrane dielectric constant,  $\epsilon_w$  = water dielectric constant). Note that some free charges (encircled) are mobile while others (in the dielectric region with  $\epsilon_m$ ) are fixed in space.

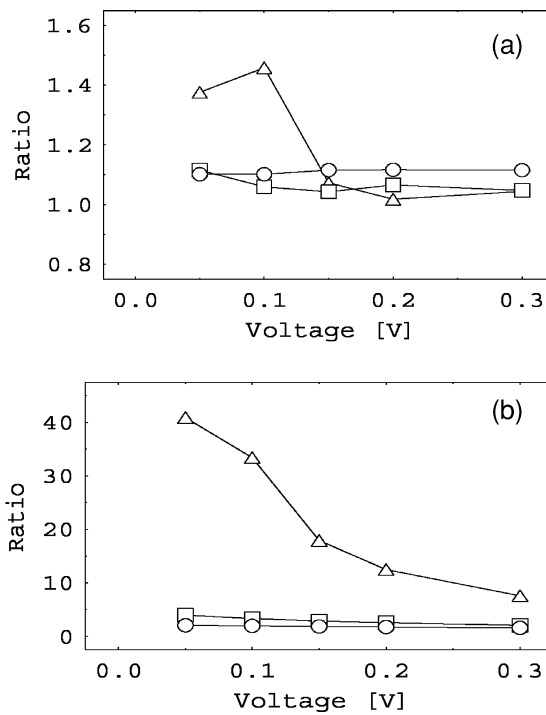


**Fig. 13.9** (a) Ratio of DSEP/BD currents as a function of voltage for three channel radii: 0.4 nm (triangles); 0.75 nm (squares); 1.2 nm (circles); (b) Ratio of PNP/BD currents for the same channels, 0.4 nm (triangles); 0.75 nm (squares); 1.2 nm (circles).

Rob D. Coalson and Maria G. Kurnikova

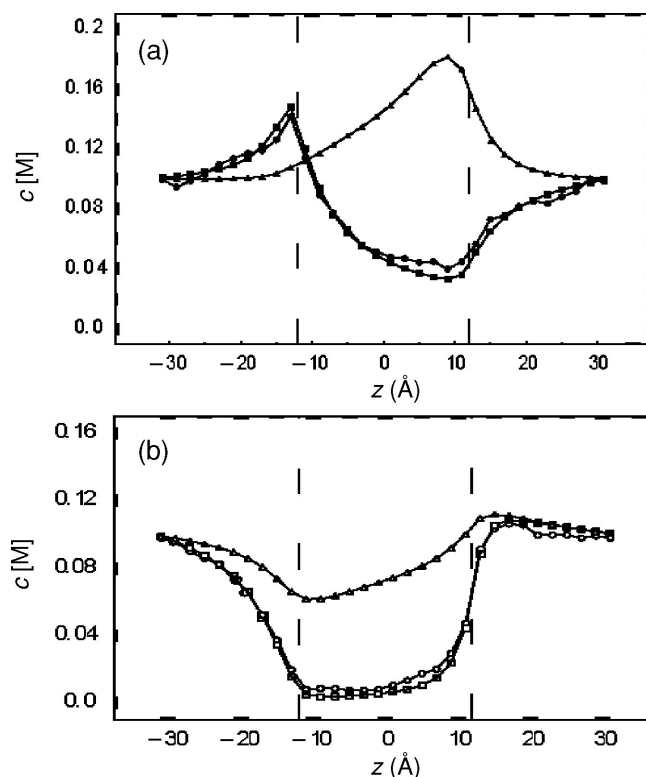


**Fig. 13.10** Mobile ion concentrations calculated by BD, DSEPNP, and PNP plotted for the  $R = 4$  Å channel at applied voltage of 0.3 V and 0.1 M reservoir concentration of salt. ~~Filled symbols are for cations; open symbols are for anions.~~ Circles show BD results, squares DSEPNP results, and triangles PNP results: (a) positive mobile ion concentration along the (channel)  $z$ -axis ( $x = 0, y = 0$ ); (b) negative mobile ion concentration along  $z$ -axis. (Vertical dashed lines delineate membrane/channel boundaries.)

## 13.6 Incorporating Effects of Channel Protein Fluctuation in PNP: PMFPNP

### 13.6.1 Free Energy of Inserting an Ion into a Channel: General Considerations

In general, calculating free energy differences in biomolecular processes is a challenging task. Several approaches have been adopted for various problems in molecular modeling. These theoretical methodologies span a wide range of molecular resolution—from estimating electrostatic free energies on a continuum level by solving the PE (Dieckmann et al., 1999; Sharp and Honig, 1990; Luty et al., 1992) to full atomistic MD simulations (Roux and Karplus, 1993; Chung et al., 1998; Kollman et al., 2000). The electrostatic free energy of transferring an ion of species

### 13. Poisson–Nernst–Planck Theory of Ion Permeation

$i$  from the bulk solution into the channel is defined by

$$\Delta G_{\text{SIP}}^i(\vec{r}) = G^{\text{complex}}(\vec{r}) - G^{\text{protein}} - G^{\text{ion}}, \quad (13.10)$$

where  $G^{\text{complex}}$  is the energy of an ion plus protein/membrane complex embedded in the solvent (water) with the ion located at a point  $\vec{r}$  inside the channel,  $G^{\text{protein}}$  is the energy of the protein/membrane system (without the ion) embedded in the same solvent and  $G^{\text{ion}}$  is the energy of a single ion in the bulk solvent. The conventional continuum electrostatic approach for calculating  $\Delta G_{\text{SIP}}^i(\vec{r})$ , based on Eq. 13.9, is reviewed in the next Section 13.5.2. A combined MD/continuum approach, which takes into account the channel flexibility, is presented in Section 13.5.3. Then, in Section 13.5.4, we present results of applying both methodologies and then simulate current through the GA channel.

#### 13.6.2 A Continuum Approach to Calculate the Electrostatic Free Energy

In the absence of external fields, the electrostatic energy  $G$  of a collection of point charges can be found as  $G = \frac{1}{2} \sum_i q_i \phi_i$ , where the summation is over all electrostatic charges  $q_i$  in the system and  $\phi_i$  is the value of the electrostatic potential at the position of charge  $i$ . The electrostatic potential  $\phi(\vec{r})$  needed to calculate  $G$  can be obtained by solving the corresponding PE:

$$\vec{\nabla} \cdot (\epsilon(\vec{r}) \vec{\nabla} \phi(\vec{r})) = -4\pi \sum_j q_j \delta(\vec{r} - \vec{r}_j), \quad (13.11)$$

supplemented by Dirichlet boundary conditions with the boundary potential set to zero. In Eq. 13.11,  $\delta$  is the 3D Dirac delta-function and  $\vec{r}_j$  is the position of charge  $q_j$ . As noted in the previous section, for channels as narrow as 4 Å in radius, a continuum description of ion permeation described by DSEPNP, i.e., Eqs. 13.1–13.3, 13.9, compares well with results of BD simulations in which ions are treated as charged particles that diffuse in an inhomogeneous dielectric medium with a prescribed diffusion coefficient (Graf et al., 2000, 2004). Such particle-based simulation models of narrow rigid channels (Chung et al., 1999; Graf et al., 2000) typically exhibit very small superlinear currents for voltages up to 200 mV. The insignificance of these currents can be traced to the presence of a DSE barrier of several  $kT$  in such pores. In contrast, real biological channels of similar size and shape exhibit substantial ionic current at low voltages, with nearly linear or sublinear current–voltage characteristics. A detailed analysis of DSEPNP and BD particle simulations suggests that the effective polarizability of the channel environment (loosely defined as the ability of the local protein environment to adjust in order to stabilize an extra electric charge) must be higher than implied by the “standard” model utilized in both BD and DSEPNP studies. A major limitation of both approaches for simulating ion motions across channels is that the protein structure is taken to be rigid (usually at its

**Rob D. Coalson and Maria G. Kurnikova**

average NMR or X-ray configuration), while in reality the protein structure responds dynamically to an ion's presence. Below, we will investigate the consequences of the rigid protein assumption.

### 13.6.3 A Combined Molecular Dynamics/Continuum Electrostatics Approach to Calculate Free Energy

$\Delta G_{\text{SIP}}^i(\vec{r})$  can in principle be found from an atomistic simulation in which all atoms on the protein, the lipid membrane and the solvent are treated explicitly. Several attempts to calculate the free energy of an ion in a GA channel by MD simulation have been reported (Roux et al., 1993; Woolf and Roux, 1997; Elber et al., 1995; Allen et al., 2004). Such calculations rely on a parameterized all-atom potential function (Elber et al., 1995; Roux and Berneche, 2002) and require complete sampling of the system configuration space. Improvements in the available parameterizations of potential functions have been slow in recent years (Roux et al., 2002). Fortunately, an alternative method of dealing with this problem, namely limited sampling of the environment configurational space, has recently been introduced (Kollman et al., 2000). Since a large portion of the configuration space required for quantitative calculation of the free energy of an ion in a solvent is due to the solvent itself, it was recently proposed (Kollman et al., 2000) that the computationally expensive sampling of solvent configurations may be replaced by considering solvent effects via an appropriate approximate averaging procedure. In this approach a full-scale equilibrium MD trajectory of the protein in an atomistic solvent is generated to sample the protein conformational space (with and without ion in the channel). The resulting sequence of  $N$  protein/water configurations is used to obtain a corresponding sequence of dielectric continuum models of these systems, in which the fixed protein charges are embedded in their corresponding atomic positions. These continuum dielectric configurations, obtained with the permeating ion fixed in a given position, are then used to compute the electrostatic free energy of inserting the ion at that position (Sharp et al., 1990). Adapting the procedure introduced in (Kollman et al., 2000), the free energy of ion-protein complex formation for ion species  $i$  is calculated as an average over all  $n = 1, \dots, N$  configurations:

$$\Delta G_{\text{SIP}}^i = \frac{1}{N} \sum_{n=1}^N \Delta G_{\text{SIP}}^{i(n)}, \quad (13.12)$$

where  $\Delta G_{\text{SIP}}^{i(n)}$  has the same meaning as in Eq. 13.10, calculated for the  $n$ th configuration. The method thus combines an MD simulation to obtain atomistic configurations of the membrane-protein-ion complex with a continuum dielectric representation of each configuration in order to obtain a simple estimate of  $\Delta G_{\text{SIP}}^{i(n)}$  for that configuration, followed by the average indicated in Eq. 13.12. This approach allows us to account for solvent effects on average, i.e., at a mean field level and to reduce the noise in the free energy calculations due to insufficient sampling of solvent configurations.

Author: Please include Roux et al., 1993 in the reference list.

Author: Please include Roux et al., 2002 in the reference list.

Author: Please include Sharp et al., 1990 in the reference list.

### 13. Poisson–Nernst–Planck Theory of Ion Permeation

The procedure described above, in which the PMF  $\Delta G_{\text{SIP}}$  is calculated via Eq. 13.12 and then used in the PNP formalism, will be termed PMF Poisson–Nernst–Planck (PMFNP). We should note that this calculation still disregards contributions to the free energy due to changes in the protein internal energy and accounts only approximately (through the temperature dependence of the dielectric functions) for entropic contributions. These missing contributions are expected to be small because deformation of the protein is minimal during the ion permeation (see Section 13.5.4), and because the changes in configurational entropy in these processes are typically small. (A similar number of degrees of freedom are constrained independent of the ion position in the channel).

#### 13.6.4 MD/Continuum Simulation of an Ion in the GA Channel

The approach outlined above was implemented in a series of calculations performed for a model GA channel. Figure 13.11 shows a 3D GA ion channel structure incorporated into a crude model of a lipid bilayer membrane, with the membrane/protein channel system solvated in water. This snapshot is taken from an MD simulation performed as described ~~in the next subsection~~. As has been noted above, the dielectric self-energy is very large for channels less than 5 Å in radius, implying the conundrum discussed above in modeling their permeability. Working with GA, the narrowest known ion channel, emphasizes the goal of understanding the permeability of such narrow channels (Dieckmann and DeGrado, 1997; Roux and MacKinnon, 1999; Graf et al., 2000; Mamonov et al., 2003).

A set of MD simulations of a single potassium ion and a single chloride ion fixed at various positions in a GA channel was performed. GA was incorporated into a slab of heavy (mass = 100 au) spheres with Lennard–Jones parameters  $\epsilon = 0.05$  kcal/mol and  $R_M = 2.5$  Å, and no partial charge. The slab of these dummy spheres represents a lipid bilayer by providing a nonpolar environment for the channel molecule. This channel-membrane model system was then immersed in a box of 738 SPC/E water molecules (Leach, 2001). Eight water molecules in random configurations were placed inside the GA pore. This system was subjected to energy minimization followed by a 200 ps constant pressure MD equilibration run at 300 K. Positions of the dummy atoms and GA atoms were constrained in space with 200 kcal/mol/Å<sup>2</sup> harmonic spring forces. After the GA-water equilibration was completed, an ion (K<sup>+</sup> or Cl<sup>-</sup>) was introduced into the channel. A force constant of 200 kcal/mol/Å<sup>2</sup> was again applied to the positions of the dummy atoms and a 10 kcal/mol/Å<sup>2</sup> force constant was applied to the backbone atoms of the GA. The energy of each system thus prepared was minimized, followed by a 30 ps equilibration period when the harmonic constraints on the GA backbone atoms were gradually reduced from 10 kcal/mol/Å<sup>2</sup> to 0.5 kcal/mol/Å<sup>2</sup>. Subsequently, 300 ps production runs were performed with constant volume dynamics at 300 K. 0.5 kcal/mol/Å<sup>2</sup> harmonic constraints were maintained on each of the backbone C and N atoms of GA. The coordinate of the ion along the channel axis ( $z$ -axis) was held fixed, while its  $x, y$  coordinates were allowed to fluctuate. The coordinates of the protein atoms

Rob D. Coalson and Maria G. Kurnikova

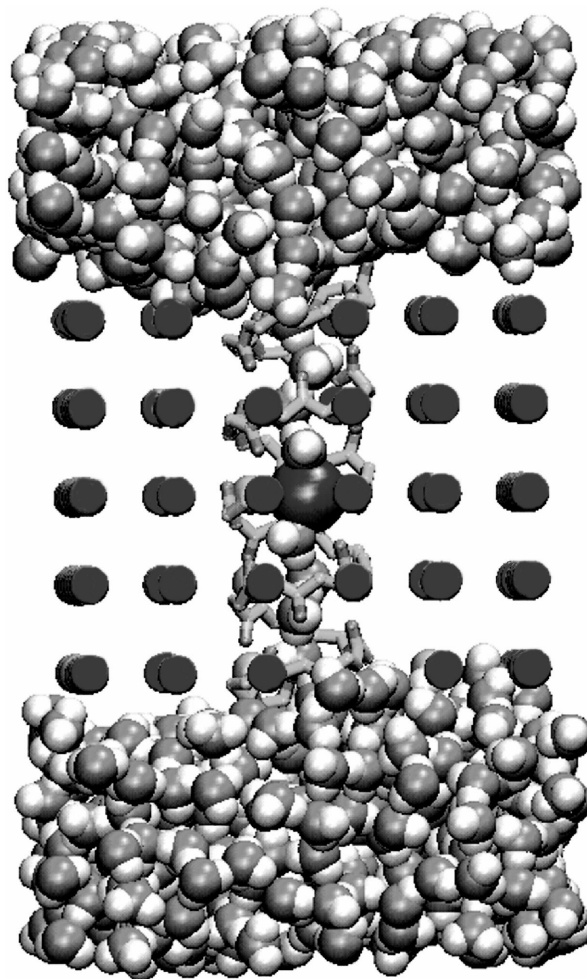


**Fig. 13.11** Snapshot of the GA channel with a  $K^+$  ion embedded in a model membrane and solvated with water after a 300 ps MD simulation as described in text. The model lipid bilayer is represented by an array of flat grey spheres (the radius of such sphere in a picture does not reflect its Lennard–Jones parameters). The  $K^+$  ion is shown as the large grey sphere in the center of the channel. Water atoms are also shown as spheres with oxygens and hydrogens colored in grey and white respectively. Only backbone atoms of the peptide chains are shown in stick representation. [For a color version of this figure, see Ref. (Mamonov et al., 2003).]

were collected every 2 ps. For every such time point along the MD trajectory the coordinates of the protein molecule and the ion were used to calculate the appropriate electrostatic free energy by solving the PE as described above.

An MD trajectory of GA without  $K^+$  was also generated as described above. All MD simulations were performed using the AMBER 6 software package and Cornell et al. force field (Cornell et al., 1995). The Lennard–Jones parameters for

*^ please make  
CLV superscript*

### 13. Poisson–Nernst–Planck Theory of Ion Permeation

the potassium ion were taken from work of (Åquist, 1990). Bonds involving hydrogen atoms were constrained via the SHAKE algorithm. A 12 Å cut-off distance was used for all nonbonded interactions. The MD time step was set to 2 fs.

For the continuum electrostatics calculations, partial charges on the GA atoms were ~~also~~ taken from the Cornell et al. force field (Cornell et al., 1995). The dielectric response profile  $\epsilon(\vec{r})$  and the positions of the partial charges represent the molecular system in a continuum representation. In this study, the dielectric constant of the membrane and the protein was set to 4, while the value characterizing both the bulk solvent and the aqueous pore was taken as 80 [for an extensive discussion of how these parameters were chosen, consult (Mamonov et al., 2003)]. In the numerical solution of the PE (Eq. 13.3), these functions are discretized on a uniform 3D grid as described in (Kurnikova et al., 1999). The radii of potassium and chlorine ions, estimated by fitting experimental enthalpies of hydration, were chosen to be  $R_{K^+} = 2.17$  Å (Dieckmann et al., 1999) and  $R_{K^-} = 1.81$  Å (Dasent, 1982). For all results reported below, the grid dimensions of the simulation box were  $151^3$  with a linear scale of 3 grid points per Å. The width of the membrane was set to 33 Å to mimic a GMO bilayer. The set of calculations described above was repeated with the potassium ion fixed at 18 different positions along one GA monomer at spatial increments of 1 Å, and the chloride ion fixed at seven different positions at spatial increments of 3 Å.

The results of the MD/free energy calculations outlined above (~~Mamonov et al., 2003~~) show the following basic features. Since GA is a tightly-bound  $\beta$ -helical structure, it is not surprising that the overall structure of peptide, embedded in an artificial lipid bilayer, do not change significantly over the course of the MD trajectory. Consequently, the DSE contribution to the overall single-particle free energy of insertion (PMF, or in the present notation, SIP) does not vary much over the course of the MD simulation. It remains close to the value associated with the static average protein configuration and provides, as expected, a large energy barrier (of about  $20kT$ ) to the passage of ions of either sign. A more interesting finding is that small local distortions of pore-lining parts of the peptide (especially carbonyl groups) significantly stabilizes cations as they move through it; cf. Fig. 13.12. This large energetic stabilization is possible because electrostatic forces are strong, and the permeating ion is very close to partially charged groups of the protein that face the aqueous pore—hence, changes in the positions of these protein groups by only fractions of an Ångstrom can change the direct Coulomb interaction with the ion by many  $kT$ . The situation here is reminiscent of polaron formation in polar crystalline solids (Kittel, 1996). In that phenomenon, an electron migrating through the crystal distorts the lattice of ions that define the crystal locally and instantaneously (on the slow time scale of the electron's migration) in such a way as to lower the overall energy of the system (ion + lattice) and thus stabilize it. The resultant species, an electron surrounded by displaced positive ions (with the negative ions distorting away from the ion), is termed a polaron. Its conduction and optical properties are altered by the “phonon cloud” that surrounds it. The case of an ion moving through a narrow protein channel is somewhat similar; again, cf. Fig. 13.12. In this system, polaronic stabilization of cations approximately cancels out the DSE barrier and allows them

o  
A

Rob D. Coalson and Maria G. Kurnikova

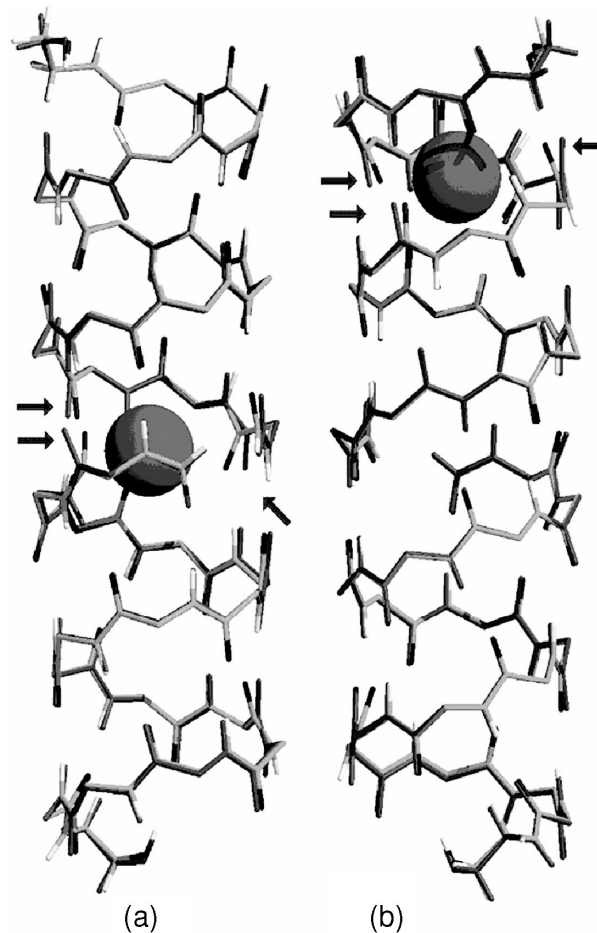


**Fig. 13.12** The average configuration of GA in MD simulation without the ion (mono color grey) is superimposed with the average configuration of GA with the  $K^+$  ion present in the simulation (mainly grey with backbone oxygens colored in black and nitrogens in white).  $K^+$  is shown as a large sphere. Arrows indicate the carbonyl oxygens that bend toward the  $K^+$  due to favorable electrostatic interactions. (a) During the MD simulation ion was in the center of the channel, (b)  $K^+$  is at 9 Å from the center of the channel, the predicted position of the binding site. [For a color version of this figure, see Ref. (Mamonov et al., 2003).]

to permeate with relative ease (as was found in primitive PNP calculations which omitted both effects!).

### 13.6.5 Application of PMFPNP to Calculate Ion Currents Through the GA Channel

Some computed PMFPNP  $I-V$  curves are shown in Fig. 13.13. The currents obtained in these calculations are typically within a factor of two of currents measured

### 13. Poisson–Nernst–Planck Theory of Ion Permeation

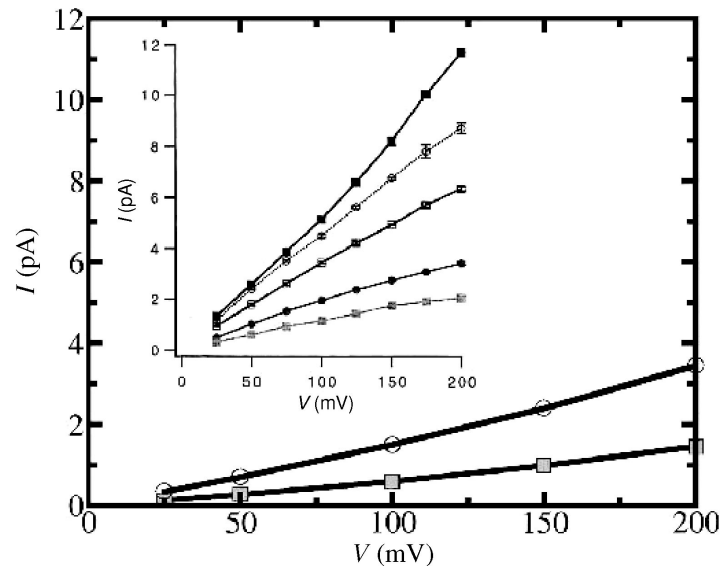


**Fig. 13.13** Current–voltage relations predicted by PMFPNP model are compared to experimental results (Busath et al., 1998) (upper left inset). Bulk KCl concentrations of 0.1 M (shaded square) and 1.0 M (open circle) were used in the simulations. The experimental curves in the inset correspond to the following concentrations of bulk KCl solutions: shaded square—0.1 M, filled circle—0.2 M, open square—0.5 M, open circle—1.0 M, and filled square—2.0 M. The analogous experimental and calculated curves are labeled with the same symbols.

experimentally (Busath et al., 1998). By adjusting the internal diffusion constant an even better (nearly perfect) fit could have been obtained. However, in these calculations, the internal ion diffusion constants were actually calculated by processing MD simulation data (based on all-atom simulations of the protein and water, plus one ion fixed inside the channel) in a standard fashion. The calculated reduction of the internal diffusion from its bulk value is comparable to that obtained by fitting (“reverse-engineering”) the internal diffusion constant (Edwards et al., 2002) to obtain agreement with experimental GA data, as discussed above.

A final important result of this study is the demonstration that PMFPNP theory is able to account for effects that are beyond the reach of primitive PNP theory, namely, saturation of ion current through the channel as the concentration of bathing solutions increases to a sufficiently high value (see Fig. 13.14). Physically, once the channel becomes filled up with ions, the dwell time of these ions before they escape from the exit side of the pore becomes the rate determining factor, rather than the rate of attempted entry into the channel (the latter being proportional to the concentration of ions in the external reservoir on the entry side, while the former is independent of this concentration). In PNP theory, a build-up of positive charge density in the channel would be expected to generate an electric field that prevents other positive ions (charge density) from entering the channel. However, in primitive PNP this positive charge has the unphysical effect of attracting negative mobile

## Rob D. Coalson and Maria G. Kurnikova

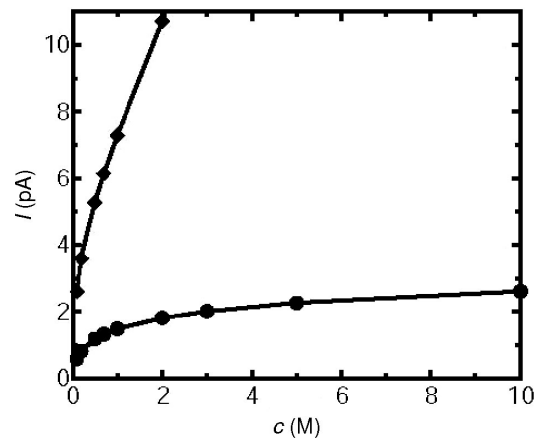


**Fig. 13.14** Current–concentration relations as predicted by PNP (diamonds) and PMFNP (circles) models. The external potential difference was set to 100 mV.

charge into the channel. ~~For example, as shown in Fig. 13.15a, in primitive PNP the concentration of cations inside the channel is always higher than in the bulk. This feature can be traced to~~ the behavior of the anions shown in Fig. 13.15c: at low electrolyte concentration anions do not enter the pore, while at high bulk electrolyte concentration (10 M), the apparent concentration of  $\text{Cl}^-$  in parts of the channel exceeds 5 M. As positive and negative charge build up in the same region (again, an unphysical process), the aqueous region of the pore is effectively rendered charge neutral, thus allowing more positive charge to enter and flow through it—the higher the bathing concentration of ions, the higher the rate of ion permeation (Fig. 13.14). In particular, Fig. 13.16a,c shows that at high concentrations the potential drop across the channel becomes roughly linear, implying that positive and negative mobile ions pile into the channel in such a way as to cancel out all electrostatic driving forces except for the applied voltage. Now we are back to the 1D NP model (essentially the GHK model discussed in Section 13.2.3), which predicts ion current proportional to bathing solution concentration. This is exactly what we see in Fig. 13.14.

In PMFNP, by contrast, the DSE added to the unfavorable protein–anion interaction potential forms a very high barrier to anion entry into the channel—even the build-up of positive ion density cannot compensate for this (see Fig 13.16d). Anions never enter into the channel (Fig. 13.15d), while cation charge continues to build up as the bathing solution salt concentration is increased (notice in Fig. 13.15b that unlike primitive PNP result [Fig. 13.15a] cation concentration build-up happens only at particular locations in the channel, which can be loosely regarded as cation binding sites), until the tendency toward greater cation flow rate into the channel with increasing electrolyte concentration is counterbalanced by the electrostatic repulsion generated by cations already in the channel—the density profile of cations in the channel saturates, ultimately causing the saturation behavior in current flow illustrated in Fig. 13.14. This saturation mechanism can be appreciated by examining

### 13. Poisson–Nernst–Planck Theory of Ion Permeation

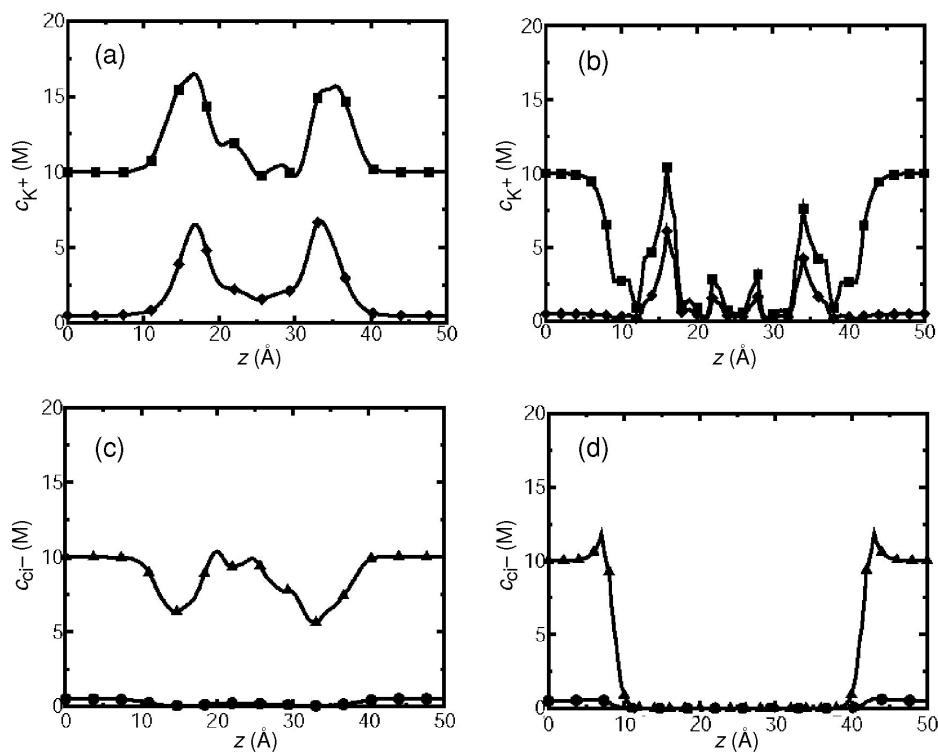


**Fig. 13.15** Ion concentration profile along the channel axis for  $K^+$  and  $Cl^-$  is plotted for two (high and low) bulk electrolyte concentrations: (a), (c) calculated using PNP; (b), (d) calculated using PMFPNP. The curves with diamonds and circles are for 0.5 M, the curves with squares and triangles are for 10 M electrolyte concentrations.

the concentration dependence of the effective driving potentials seen by anions vs. cations, as illustrated in Fig. 13.16a,c for primitive PNP and in Fig. 13.16b,d for PMFPNP.

### 13.7 Conclusions and Outlook

Three-dimensional PNP Theory has an intuitive appeal due to its conceptual simplicity. It relies on a caricature of the microscopic world in which background media are treated as dielectric slabs and the primary particles of interest, mobile ions like  $Na^+$  and  $Cl^-$ , are “smeared out” into a continuous charge distribution. The polarization of this mobile charge distribution in response to concentration gradients in boundary reservoirs and electrostatic forces arising from both internal (ion–ion, ion–protein, etc.) and external (electrode-generated) sources is described in terms of drift–diffusion equations. These are coupled naturally to the PE of electrostatics which must be utilized to calculate the relevant electric fields (self-consistently

## Rob D. Coalson and Maria G. Kurnikova

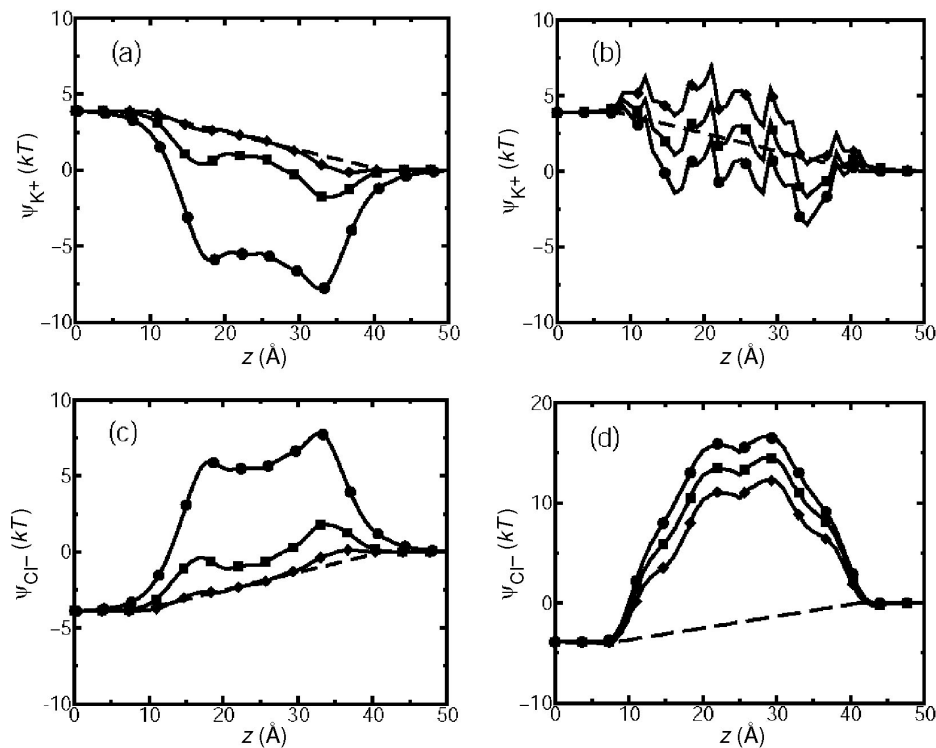


**Fig. 13.16**  $\psi_i(\vec{r})$  profile along the channel axes for  $K^+$  and  $Cl^-$  is plotted for several bulk electrolyte concentrations and 100 mV applied voltage: (a), (c) calculated using PNP; (b), (d) calculated using PMF. The curve with circles is for 0 M, the curve with squares is for 0.5 M and the curve with diamonds is for 10 M electrolyte concentrations. The dashed line is the result of the calculation in which protein molecule had no partial charges on the atoms. It corresponds to the linear ramp potential caused by the high resistivity of the membrane.

with the solution of the drift–diffusion equations). This “engineering flavor” is transferred to numerical solution techniques, e.g., PDE solvers relying on well-developed finite difference or finite element methods. As advances in these techniques (such as variable meshes and multigriding (Beck, 1997; Tsonchev et al., 2004)) become available, 3D PNP solvers will surely become fast enough that they can be distributed as software, analogous, say, to the FEMLAB program (FEMLAB, 2004) that solves standard PDEs of many types. In the context of understanding structure–function relations in biological ion channels, 3D PNP solvers may soon serve as a Computer Assisted Design (CAD) tool, which allows the user to vary inputs and get accurate output solutions (within the range of validity of PNP theory) quickly. One can imagine high throughput scanning, for example, of the effects on current flow through an ion channel due to changes in critical amino acids. Such calculations could then guide experimentalists who wish to generate the mutated channels (using site-directed mutagenesis techniques) to alter channel function.

### 13. Poisson–Nernst–Planck Theory of Ion Permeation

Before getting carried away with the potential uses of 3D PNP solvers, we should bear in mind the inherent restrictions of the theory. The caricature outlined in the preceding paragraph may simply be unrealistic for treating certain properties of certain ion channels. Many ion channels have a narrow segment through which ions can only flow in single file fashion (this is a common feature of ion channel selectivity filters, for example). These regions are characterized by electrostatic traps (binding sites), where ions reside, one ion per binding site, temporarily. A site-bound ion is then knocked out of its binding site (and through the channel) by another ion entering the channel. These kinds of mechanisms are not included in primitive PNP. We have seen above that the consequences of many such effects (e.g., saturation of ion current with increasing bathing solution concentration) can in fact be attained from modified versions of PNP, but this may be due to judicious cancellation of errors in a description which is fundamentally inadequate to accurately describe the underlying dynamics.

Despite these concerns, we expect that in years to come PNP type theories will continue to play a useful role in computing and understanding the kinetics of ion permeation through biological channels, especially in wider channels (Im *et al.*, 2002; Noskov *et al.*, 2004), synthetic channels [e.g., based on carbon nanotubes (Hummer *et al.*, 2001)], etc. Consider the fate of other continuum electrostatic theories which describe dynamical processes in solution, such as the Born theory of solvation (Dill and Bromberg, 2003) and the Marcus theory of electron transfer (Marcus, 1956, 1965). Although they are much criticized for not possessing sufficient microscopic detail, they have proven remarkably robust in estimating, semi-quantitatively, the complicated phenomena that they were developed to model, with only back of the envelope calculations. Thus they remain invaluable to the present day. We suspect that the same will prove true of electrodiffusion theories, and PNP in particular, for understanding ion permeation through nano-pores.

**Author: Please include Im *et al.*, 2002 in the reference list.**

### Acknowledgments

We thank our collaborators A. Nitzan, P. Graf, A. Cárdenas, A. Mamonov, and M. Cheng for sharing their insights on this subject with us over the years. Our work on 3D PNP theory and its application to ion permeation through biological channels has been supported by grants from PRF, NSF, NIH, and ARO.

### References

- Aksimentiev, A. and K. Schulten. 2005. Imaging alpha-hemolysin with molecular dynamics: Ionic conductance, osmotic permeability, and the electrostatic potential map. *Biophys. J.* 88:3745–3761.
- Allen, T.W., O.S. Andersen, and B. Roux. 2004. Energetics of ion conduction through the gramicidin channel. *Proc. Natl. Acad. Sci. USA* 101:117–122.

**Rob D. Coalson and Maria G. Kurnikova**

- Åquist, J. 1990. Ion water interaction potentials derived from free-energy perturbation simulations. *J. Phys. Chem.* 94:8021–8024.
- Arsen'ev, A.S., A.L. Lomize, I.L. Barsukov, and V.F. Bystrov. 1986. Gramicidin A transmembrane ion-channel. Three-dimensional structure reconstruction based on NMR spectroscopy and energy refinement. *Biol. Membr.* 3:1077–1104.
- Barcilon, V. 1992. Ion flow through narrow membrane channels. 1. *SIAM J. Appl. Math.* 52:1391–1404.
- Barcilon, V., D.P. Chen, and R.S. Eisenberg. 1992. Ion flow through narrow membrane channels. 2. *SIAM J. Appl. Math.* 52:1405–1425.
- Beck, T.L. 1997. Real-space multigrid solution of electrostatics problems and the Kohn-Sham equations. *Int. J. Quantum Chem.* 65:477–486.
- Bockris, J.O., and A.K.N. Reddy. 1998. *Modern Electrochemistry 1: Ionics*. Premium Press, New York.
- Burykin, A., C.N. Schutz, J. Vill, and A. Warshel. 2002. Simulations of ion current in realistic models of ion channels: The KcsA potassium channel. *Proteins Struct. Funct. Genet.* 43:265–280.
- Busath, D.D., C.D. Thulin, R.W. Hendershot, L.R. Phillips, P. Maughan, C.D. Cole, N.C. Bingham, S. Morrison, L.C. Baird, R.J. Hendershot, M. Cotten, and T.A. Cross. 1998. Noncontact dipole effects on channel permeation. I. Experiments with (5F-indole)trp(13) gramicidin A channels. *Biophys. J.* 75:2830–2844.
- Cardenas, A.E., R.D. Coalson, and M.G. Kurnikova. 2000. Three-dimensional Poisson–Nernst–Planck theory studies: Influence of membrane electrostatics on gramicidin A channel conductance. *Biophys. J.* 79:80–93.
- Chandler, D. 1987. *Introduction to Modern Statistical Mechanics*. Oxford University Press, New York, 274pp.
- Chandrasekhar, S. 1943. Stochastic problems in physics and astronomy. *Rev. Mod. Phys.* 15:1–89.
- Chen, D.P., and R. Eisenberg. 1993a. Charges, currents, and potentials in ionic channels of one conformation. *Biophys. J.* 64:1405–1421.
- Chen, D.P., and R.S. Eisenberg. 1993b. Flux, coupling, and selectivity in ionic channels of one conformation. *Biophys. J.* 65:727–746.
- Cheng, M.H., M. Cascio, and R.D. Coalson. 2005. Theoretical studies of the M2 transmembrane segment of the glycine receptor. Models of the open pore structure and current–voltage characteristics. *Biophys. J.* 88:110a.
- Chung, S.H., T.W. Allen, M. Hoyles, and S. Kuyucak. 1999. Permeation of ions across the potassium channel: Brownian dynamics studies. *Biophys. J.* 77:2517–2533.
- Chung, S.H., T.W. Allen, and S. Kuyucak. 2002. Conducting-state properties of the KcsA potassium channel from molecular and Brownian dynamics simulations. *Biophys. J.* 82:628–645.
- Chung, S.H., M. Hoyles, T. Allen, and S. Kuyucak. 1998. Study of ionic currents across a model membrane channel using Brownian dynamics. *Biophys. J.* 75:793–809.
- Chung, S.H., and S. Kuyucak. 2002. Recent advances in ion channel research. *BBA Biomembr.* 1565:267–286.

### 13. Poisson–Nernst–Planck Theory of Ion Permeation

- Coalson, R.D., and T.L. Beck. 1998. Numerical Methods for Solving Poisson and Poisson–Boltzman type Equations. John Wiley & Sons, pp. 2086–2100.
- Coalson, R.D., and M.G. Kurnikova. 2005. Poisson–Nernst–Planck theory approach to the calculation of current through biological ion channels. *IEEE Trans. Nanobiosci.* 4:81–93.
- Cornell, W.D., P. Cieplak, C.I. Bayly, I.R. Gould, K.M. Merz, D.M. Ferguson, D.C. Spellmeyer, T. Fox, J.W. Caldwell, and P.A. Kollman. 1995. A 2nd generation force-field for the simulation of protein, nucleic-acid, and organic-molecules. *J. Am. Chem. Soc.* 117:5179–5197.
- Corry, B., S. Kuyucak, and S.H. Chung. 2003. Dielectric self-energy in Poisson–Boltzmann and Poisson–Nernst–Planck models of ion channels. *Biophys. J.* 84:3594–3606.
- Crozier, P.S., D. Hencclerson, R.L. Rowley, and D.D. Busath. 2001a. Model channel ion currents in NaCl-extended simple point charge water solution with applied-field molecular dynamics. *Biophys. J.* 81:3077–3089.
- Crozier, P.S., R.L. Rowley, N.B. Holladay, D. Henderson, and D.D. Busath. 2001b. Molecular dynamics simulation of continuous current flow through a model biological membrane channel. *Phys. Rev. Lett.* 86:2467–2470.
- Dasent, W.E. 1982. Inorganic Energetics, 2nd Ed. Cambridge University Press, New York.
- Dieckmann, G.R., and W.F. DeGrado. 1997. Modeling transmembrane helical oligomers. *Curr. Opin. Struct. Biol.* 7:486–494.
- Dieckmann, G.R., J.D. Lear, Q.F. Zhong, M.L. Klein, W.F. DeGrado, and K.A. Sharp. 1999. Exploration of the structural features defining the conduction properties of a synthetic ion channel. *Biophys. J.* 76:618–630.
- Dill, K.A., and S. Bromberg. 2003. Molecular Driving Forces: Statistical Thermodynamics in Chemistry and Biology. Garland Science, New York. 666pp.
- Doi, M. 1996. Introduction to Polymer Physics. Clarendon Press, Oxford. 120pp.
- Edwards, S., B. Corry, S. Kuyucak, and S.H. Chung. 2002. Continuum electrostatics fails to describe ion permeation in the gramicidin channel. *Biophys. J.* 83:1348–1360.
- Elber, R., D. Rojewska, D.P. Chen, and R.S. Eisenberg. 1995. Sodium in gramicidin – an example of a permion. *Biophys. J.* 68:906–924.
- FEMLAB: Multiphysics modeling. 2004. <http://www.comsol.com/products/femlab>.
- Gillespie, D., L. Xu, Y. Wang, and G. Meissner. 2005. (De)constructing the ryanodine receptor: Modeling ion permeation and selectivity of the calcium release channel. *J. Phys. Chem. B* 109:15598–15610.
- Gilson, M.K., T.P. Straatsma, J.A. McCammon, D.R. Ripoll, C.H. Faerman, P.H. Axelsen, I. Silman, and J.L. Sussman. 1994. Open “back door” in a molecular dynamics simulation of acetylcholinesterase. *Science* 263:1276–1278.
- Graf, P., M. Kurnikova, R. Coalson, and A. Nitzan. 2004. Comparison of dynamic lattice Monte Carlo simulations and the dielectric self-energy Poisson–Nernst–Planck continuum theory for model ion channels. *J. Phys. Chem. B* 108:2006–2015.

**Au: Please  
provide the  
location of the  
publisher.**

**Rob D. Coalson and Maria G. Kurnikova**

- Graf, P., A. Nitzan, M.G. Kurnikova, and R.D. Coalson. 2000. A dynamic lattice Monte Carlo model of ion transport in inhomogeneous dielectric environments: Method and implementation. *J. Phys. Chem. B* 104:12324–12338.
- Hille, B. 1992. *Ionic Channels of Excitable Membranes*. Sinauer Associates, Cambridge, NY. 814pp.
- Hollerbach, U., D.P. Chen, D.D. Busath, and B. Eisenberg. 2000. Predicting function from structure using the Poisson–Nernst–Planck equations: Sodium current in the gramicidin A channel. *Langmuir* 16:5509–5514.
- Hummer, G., J.C. Rasaiah, and J.P. Noworyta. 2001. Water conduction through the hydrophobic channel of a carbon nanotube. *Nature* 414:188–190.
- Im, W., and B. Roux. 2002. Ions and counterions in a biological channel: A molecular dynamics simulation of OmpF porin from *Escherichia coli* in an explicit membrane with 1 M KCl aqueous salt solution. *J. Mol. Biol.* 319:1177–1197.
- Ise, N., and H. Yoshida. 1996. Paradoxes of the repulsion-only assumption. *Acc. Chem. Res.* 29:3–5.
- Kittel, C. 1996. *Introduction to Solid State Physics*, 7th Ed. John Wiley & Sons, New York, 665pp.
- Kollman, P.A., I. Massova, C. Reyes, B. Kuhn, S.H. Huo, L. Chong, M. Lee, T. Lee, Y. Duan, W. Wang, O. Donini, P. Cieplak, J. Srinivasan, D.A. Case, and T.E. Cheatham. 2000. Calculating structures and free energies of complex molecules: Combining molecular mechanics and continuum models. *Acc. Chem. Res.* 33:889–897.
- Kurnikova, M.G., R.D. Coalson, P. Graf, and A. Nitzan. 1999. A lattice relaxation algorithm for three-dimensional Poisson–Nernst–Planck theory with application to ion transport through the gramicidin A channel. *Biophys. J.* 76:642–656.
- Leach, A.R. 2001. *Molecular Modelling: Principles and Applications*, 2nd Ed. Prentice Hall, Harlow, England. 744pp.
- Luty, B.A., M.E. Davis, and J.A. McCammon. 1992. Solving the finite-difference non-linear Poisson–Boltzmann equation. *J. Comp. Chem.* 13:1114–1118.
- Lynden-Bell, R.M., and J.C. Rasaiah. 1996. Mobility and solvation of ions in channels. *J. Chem. Phys.* 105:9266–9280.
- Mamonov, A.B., R.D. Coalson, A. Nitzan, and M.G. Kurnikova. 2003. The role of the dielectric barrier in narrow biological channels: A novel composite approach to modeling single-channel currents. *Biophys. J.* 84:3646–3661.
- Marcus, R.A. 1956. On the theory of oxidation–reduction reactions involving electron transfer. I. *J. Chem. Phys.* 24:966–978.
- Marcus, R.A. 1965. On the theory of electron-transfer reactions. VI. Unified treatment for homogeneous and electrode reactions. *J. Chem. Phys.* 43:679–701.
- Marion, J.B. 1965. *Classical Electromagnetic Radiation*. Academic Press, New York, 479pp.
- Mashl, R.J., Y.Z. Tang, J. Schnitzer, and E. Jakobsson. 2001. Hierarchical approach to predicting permeation in ion channels. *Biophys. J.* 81:2473–2483.
- McQuarrie, D.A. 1976. *Statistical Mechanics*, Harper Collins Publishers, New York, 641pp.

### 13. Poisson–Nernst–Planck Theory of Ion Permeation

- Noskov, S. Y., W. Im, and B. Roux. 2004. Ion permeation through the alpha-hemolysin channel: Theoretical studies based on Brownian dynamics and Poisson–Nernst–Planck electrodiffusion theory. *Biophys. J.* 87:2299–2309.
- Peyghambarian, N., S.W. Koch, and A. Mysyrowicz. 1993. Introduction to Semiconductor Optics. Prentice Hall, Englewood Cliffs, NJ.
- Press, W.H., B.P. Flannery, S.A. Teukolsky, and W.T. Vetterling. 1986. Numerical Recipes. Cambridge University Press, New York, 848pp.
- Rostovtseva, T.K., V.M. Aguilera, I. Vodyanoy, S.M. Bezrukov, and V.A. Parsegian. 1998. Membrane surface-charge titration probed by gramicidin A channel conductance. *Biophys. J.* 75:1783–1792.
- Roux, B., and S. Berneche. 2002. On the potential functions used in molecular dynamics simulations of ion channels. *Biophys. J.* 82:1681–1684.
- Roux, B., and R. MacKinnon. 1999. The cavity and pore helices the KcsA K<sup>+</sup> channel: Electrostatic stabilization of monovalent cations. *Science* 285:100–102.
- Roux, B., and M. Karplus. 1993. Ion transport in the Gramicidin channel: Free energy of the solvated ion in a model membrane. *J. Am. Chem. Soc.* 115:3250–3260.
- Schuss, Z., B. Nadler, and R.S. Eisenberg. 2001. Derivation of Poisson and Nernst–Planck equations in a bath and channel from a molecular model. *Phys. Rev. E* 64:036116:1–14.
- Sharp, K.A., and B.H. Honig. 1990. Electrostatic interactions in macromolecules— theory and applications. *Ann. Rev. Biophys. Biophys. Chem.* 19:301–332.
- Sten-Knudsen, O. 1978. Passive transport processes. In: Membrane Transport in Biology. G. Giebisch, D.C. Tosteson, and H.H. Ussing, editors. Springer-Verlag, New York, pp. 5–114.
- Tsonchev, S., R.D. Coalson, A. Liu, and T.L. Beck. 2004. Flexible polyelectrolyte simulations at the Poisson–Boltzmann level: A comparison of the kink-jump and multigrid configurational-bias Monte Carlo methods. *J. Chem. Phys.* 120:9817–9821.
- Wang, Y., L. Xu, D.A. Pasek, D. Gillespie, and G. Meissner. 2005. Probing the role of negatively charged amino acid residues in ion permeation of skeletal muscle ryanodine receptor. *Biophys. J.* 89:256–265.
- Wissenburg, P., T. Odjik, P. Cirkel, and M. Mandel. 1995. Multimolecular aggregation of mononucleosomal DNA in concentrated isotropic solutions. *Macromol* 28:2315–2328.
- Wolf, T.B., and B. Roux. 1997. The binding site of sodium in the gramicidin A channel: Comparison of molecular dynamics with solid-state NMR data. *Biophys. J.* 72:1930–1945.

